

- bladder cancer in humans. *Biochem. Biophys. Res. Commun.*, **277**: 776–780 (2000).
- 14) Imaoka, S., Yoneda, Y., Matsuda, T., Degawa, M., Fukushima, S. and Funae, Y.: Mutagenic activation of urinary bladder carcinogens by CYP4B1 and the presence of CYP4B1 in bladder mucosa. *Biochem. Pharmacol.*, **54**: 677–683 (1997).
 - 15) Vanderslice, R. R., Boyd, J. A., Eling, T. E. and Philpot, R. M.: The cytochrome P-450 monooxygenase system of rabbit bladder mucosa: enzyme components and isozyme 5-dependent metabolism of 2-aminofluorene. *Cancer Res.*, **45**: 5851–5858 (1985).
 - 16) Hiratsuka, M., Nozawa, H., Konno, Y., Saito, T., Konno, S. and Mizugaki, M.: Human CYP4B1 gene in the Japanese population analyzed by denaturing HPLC. *Drug Metab. Pharmacokin.*, **19**: 114–119 (2004).
 - 17) Sasaki, T., Horikawa, M., Orikasa, K., Sato, M., Arai, Y., Mitachi, Y., Mizugaki, M., Ishikawa, M. and Hiratsuka, M.: Possible relationship between the risk of Japanese bladder cancer cases and the CYP4B1 genotype. *Jpn. J. Clin. Oncol.*, **38**: 634–640 (2008).
 - 18) Falany, C. N.: Enzymology of human cytosolic sulfotransferases. *FASEB J.*, **11**: 206–216 (1997).
 - 19) Richard, K., Hume, R., Kaptein, E., Stanley, E. L., Visser, T. J. and Coughtrie, M. W.: Sulfation of thyroid hormone and dopamine during human development: ontogeny of phenol sulfotransferases and arylsulfatase in liver, lung, and brain. *J. Clin. Endocrinol. Metab.*, **86**: 2734–2742 (2001).
 - 20) Arslan, S., Silig, Y. and Pinarbasi, H.: An investigation of the relationship between SULT1A1 Arg(213)His polymorphism and lung cancer susceptibility in a Turkish population. *Cell Biochem. Funct.*, **27**: 211–215 (2009).
 - 21) Liang, G., Miao, X., Zhou, Y., Tan, W. and Lin, D.: A functional polymorphism in the SULT1A1 gene (G638A) is associated with risk of lung cancer in relation to tobacco smoking. *Carcinogenesis*, **25**: 773–778 (2004).
 - 22) Kihara, M. and Noda, K.: Risk of smoking for squamous and small cell carcinomas of the lung modulated by combinations of CYP1A1 and GSTM1 gene polymorphisms in a Japanese population. *Carcinogenesis*, **16**: 2331–2336 (1995).
 - 23) Pinarbasi, H., Silig, Y., Cetinkaya, O., Seyfikli, Z. and Pinarbasi, E.: Strong association between the GSTM1-null genotype and lung cancer in a Turkish population. *Cancer Genet. Cytogenet.*, **146**: 125–129 (2003).
 - 24) Oscarson, M., McLellan, R. A., Gullsten, H., Yue, Q. Y., Lang, M. A., Bernal, M. L., Sinues, B., Hirvonen, A., Raunio, H., Pelkonen, O. and Ingelman-Sundberg, M.: Characterisation and PCR-based detection of a CYP2A6 gene deletion found at a high frequency in a Chinese population. *FEBS Lett.*, **448**: 105–110 (1999).
 - 25) Tamaki, Y., Honda, M., Muroi, Y., Arai, T., Sugimura, H., Matsubara, Y., Kanno, S., Ishikawa, M., Hirasawa, N. and Hiratsuka, M.: Novel single nucleotide polymorphism of the CYP2A13 gene in Japanese individuals. *Drug Metab. Pharmacokin.*, **in press** (2011).
 - 26) Abdel-Rahman, S. Z., el-Zein, R. A., Anwar, W. A. and Au, W. W.: A multiplex PCR procedure for polymorphic analysis of GSTM1 and GSTT1 genes in population studies. *Cancer Lett.*, **107**: 229–233 (1996).
 - 27) Timofeeva, M. N., Kropp, S., Sauter, W., Beckmann, L., Rosenberger, A., Illig, T., Jager, B., Mittelstrass, K., Dienemann, H., Bartsch, H., Bickeboller, H., Chang-Claude, J. C., Risch, A. and Wichmann, H. E.: CYP450 polymorphisms as risk factors for early-onset lung cancer: gender-specific differences. *Carcinogenesis*, **30**: 1161–1169 (2009).
 - 28) To-Figueras, J., Gene, M., Gomez-Catalan, J., Galan, M. C., Fuentes, M., Ramon, J. M., Rodamilans, M., Huguet, E. and Corbella, J.: Glutathione S-transferase M1 (GSTM1) and T1 (GSTT1) polymorphisms and lung cancer risk among Northwestern Mediterraneans. *Carcinogenesis*, **18**: 1529–1533 (1997).

Functional Characterization of CYP2B6 Allelic Variants in Demethylation of Antimalarial Artemether

Masashi Honda, Yuka Muroi, Yuichiro Tamaki, Daisuke Saigusa, Naoto Suzuki, Yoshihisa Tomioka, Yoichi Matsubara, Akifumi Oda, Noriyasu Hirasawa, and Masahiro Hiratsuka

Laboratory of Pharmacotherapy of Life-Style Related Diseases (M.H., Y.Mu., Y.Ta., N.H., M.H.) and Laboratory of Oncology, Pharmacy Practice and Sciences, Graduate School of Pharmaceutical Sciences, Tohoku University, Sendai, Japan (D.S., N.S., Y.To.); Department of Medical Genetics, Tohoku University School of Medicine, Sendai, Japan (Y.Ma.); and Faculty of Pharmaceutical Sciences, Tohoku Pharmaceutical University, Sendai, Japan (A.O.)

Received May 5, 2011; accepted July 11, 2011

ABSTRACT:

Artemether (AM) is one of the most effective antimalarial drugs. The elimination half-life of AM is very short, and it shows large interindividual variability in pharmacokinetic parameters. The aim of this study was to identify cytochrome P450 (P450) isozymes responsible for the demethylation of AM and to evaluate functional differences between 26 CYP2B6 allelic variants in vitro. Of 14 recombinant P450s examined in this study, CYP2B6 and CYP3A4 were primarily responsible for production of the desmethyl metabolite dihydroartemisinin. The intrinsic clearance (V_{max}/K_m) of CYP2B6 was 6-fold higher than that of CYP3A4. AM demethylation activity was correlated with CYP2B6 protein levels ($P = 0.004$); however, it was not correlated with CYP3A4 protein levels ($P = 0.27$) in human liver microsomes. Wild-type CYP2B6.1 and 25 CYP2B6 allelic variants (CYP2B6.2-CYP2B6.21 and CYP2B6.23-

CYP2B6.27) were heterologously expressed in COS-7 cells. In vitro analysis revealed no enzymatic activity in 5 variants (CYP2B6.8, CYP2B6.12, CYP2B6.18, CYP2B6.21, and CYP2B6.24), lower activity in 7 variants (CYP2B6.10, CYP2B6.11, CYP2B6.14, CYP2B6.15, CYP2B6.16, CYP2B6.20, and CYP2B6.27), and higher activity in 4 variants (CYP2B6.2, CYP2B6.4, CYP2B6.6, and CYP2B6.19), compared with that of wild-type CYP2B6.1. In kinetic analysis, 3 variants (CYP2B6.2, CYP2B6.4, and CYP2B6.6) exhibited significantly higher V_{max} , and 3 variants (CYP2B6.14, CYP2B6.20 and CYP2B6.27) exhibited significantly lower V_{max} compared with that of CYP2B6.1. This functional analysis of CYP2B6 variants could provide useful information for individualization of antimalarial drug therapy.

Introduction

Malaria is a very serious problem in many countries, and there are more than 200 million cases that result in approximately 1 million deaths worldwide each year (World Health Organization, World Malaria Report 2009, http://www.who.int/malaria/world_malaria_report_2009/en/index.html). The management of malaria has traditionally relied on monotherapy with quinolines such as quinine, mefloquine, and chloroquine. However, the widespread and excessive use of these agents has resulted in drug resistance (Wernsdorfer, 1991; Price and Nosten, 2001; Le Bras and Durand, 2003). In several studies, artemisinins, unique sesquiterpene lactone endoperoxides, have been used in areas with multidrug-resistant *Plasmodium falciparum* malaria (Woodrow et al., 2005; Gautam et al., 2009; World Health Organization, 2010).

This work was supported by the Japan Society for the Promotion of Science [KAKENHI 20590154] and in part by the Smoking Research Foundation.

Article, publication date, and citation information can be found at <http://dmd.aspetjournals.org>.

doi:10.1124/dmd.111.040352.

Artemisinin is a natural antimalarial agent derived from the Chinese medicinal plant *Artemisia annua* (Klayman, 1985). The artemisinin derivative artemether (AM) is the most effective antimalarial drug. AM has a fast onset of action, therapeutic efficacy against multidrug-resistant malaria, and few side effects, although neurotoxicity has been observed in experimental mammals (Hien and White, 1993; Brewer et al., 1994). AM is mainly converted to dihydroartemisinin (DHA) (Fig. 1), a desmethyl metabolite that contributes to the majority of the antimalarial activity. The conversion of AM to DHA is catalyzed by cytochrome P450 (P450) (van Agtmael et al., 1999b,c; Navaratnam et al., 2000). However, the elimination half-life of AM is very short, and it shows large interindividual variability in pharmacokinetic parameters (Na Bangchang et al., 1994; Mordi et al., 1997; van Agtmael et al., 1999a; Lefèvre et al., 2002; Ali et al., 2010; Mwesigwa et al., 2010).

The P450 isozymes CYP2B6 and CYP3A4 are thought to catalyze AM demethylation (Navaratnam et al., 2000). In contrast, it has been reported that CYP2D6 and CYP2C19 make no major contribution to this reaction (van Agtmael et al., 1998), and the role of other P450s remains unclear. CYP2B6 plays a major role in the biotransformation of several therapeutically important drugs, including cyclophosph-

ABBREVIATIONS: AM, artemether; DHA, dihydroartemisinin; P450, cytochrome P450; ART, artemisinin; LC, liquid chromatography; MS/MS, tandem mass spectrometry.

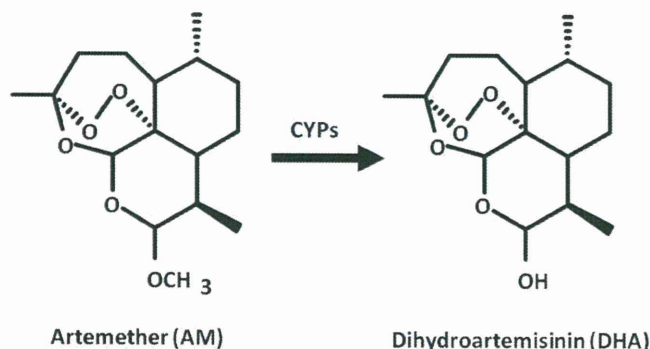


Fig. 1. Metabolic pathway of artemether to dihydroartemisinin by P450 enzymes.

amide, bupropion, selegiline, efavirenz, nevirapine, and methadone (Roy et al., 1999; Hesse et al., 2000; Hidestrand et al., 2001; Salonen et al., 2003). Many genetic polymorphisms in the *CYP2B6* gene have been reported, and these are thought to be responsible for interindividual and interethnic differences in responses to *CYP2B6* substrate drugs [Zanger et al., 2007; Human Cytochrome P450 (CYP) Allele Nomenclature Committee, 2008; Mo et al., 2009]. In the case of chemotherapy using cyclophosphamide, the increasing enzymatic activity of *CYP2B6* variants can be associated with the increased blood concentration of the active metabolite of the drug, resulting in a heightened risk of side effects (Xie et al., 2003, 2006; Nakajima et al., 2007).

Several functional analyses of *CYP2B6* variant proteins, using an in vitro expression system, have been reported. Watanabe et al. (2010) characterized the functional relevance of many *CYP2B6* variants, including *CYP2B6.1* to *CYP2B6.28*, using 7-ethoxy-4-trifluoromethylcoumarin and selegiline as substrates, and reported that *CYP2B6.8*, *CYP2B6.11*, *CYP2B6.12*, *CYP2B6.13*, *CYP2B6.15*, *CYP2B6.18*, *CYP2B6.21*, *CYP2B6.24*, and *CYP2B6.28* were inactive with regard to these compounds. These results were consistent with those of a number of in vitro studies using bupropion as a substrate. In contrast, *CYP2B6.16*, *CYP2B6.19*, and *CYP2B6.27* exhibited activity toward 7-ethoxy-4-trifluoromethylcoumarin and inability to detect selegiline metabolism. Several researchers have reported that these *CYP2B6* variants exhibited decreased protein expression/activity when bupropion was used as the *CYP2B6* substrate (Lang et al., 2004; Klein et al., 2005; Wang et al., 2006; Rotger et al., 2007). These results suggest that some allelic variants of *CYP2B6* are associated with a substrate-dependent decrease in the catalytic properties of the enzyme. To date, there have been no reports of functional characterization of *CYP2B6* variants in relation to AM demethylation activity.

In this study, we performed an in vitro analysis of 14 P450s (*CYP1A1*, *CYP1A2*, *CYP1B1*, *CYP2A6*, *CYP2B6*, *CYP2C8*, *CYP2C9*, *CYP2C19*, *CYP2D6*, *CYP2E1*, *CYP2J2*, *CYP3A4*, *CYP3A5*, and *CYP4A11*) to identify isoforms responsible for AM demethylation and evaluated functional differences among 26 *CYP2B6* allelic variants (Fig. 2).

Materials and Methods

Chemicals. AM, DHA, and artemisinin (ART) were purchased from Tokyo Chemical Industry Corporation (Tokyo, Japan). Recombinant *CYP1A1*, *CYP2A6*, *CYP2B6*, *CYP2C8*, *CYP2D6*, *CYP2J2*, and *CYP4A11* Supersomes were purchased from BD Biosciences (Woburn, MA). *CYP1A2*, *CYP2C9*, *CYP2E1*, *CYP3A4*, and *CYP3A5* Baculosomes were purchased from Invitrogen (Carlsbad, CA). NADPH was obtained from Oriental Yeast (Tokyo, Japan). Protease Inhibitor Cocktail Set III was purchased from Merck Chemicals (Darmstadt, Germany). Methanol (CH_3OH) and acetonitrile (CH_3CN) of LC-mass spectrometry grade were obtained from Kanto Chemical (Tokyo, Japan). Ammonium formate (HCOONH_4) and formic acid (HCOOH) of LC-

mass spectrometry grade were obtained from Wako Pure Chemical Industries (Tokyo, Japan).

DHA stock solution (5 mM) was prepared in $\text{CH}_3\text{CN}/\text{H}_2\text{O}$ [50:50 (v/v)], and working solutions (1.0, 2.0, 5.0, 10, 25, 50, 100, and 200 μM) were prepared from the stock solution. These solutions were further diluted in 50 mM potassium phosphate buffer, pH 7.4, and the final calibration curves were obtained with 0.1, 0.2, 0.5, 1.0, 2.5, 5.0, 10, and 20 μM solutions. Working solutions (100 μl) were prepared in 1.5-ml plastic tubes, and 100 μl of CH_3OH , 5 μl of internal standard (ART at 100 μM), and 100 μl of H_2O were

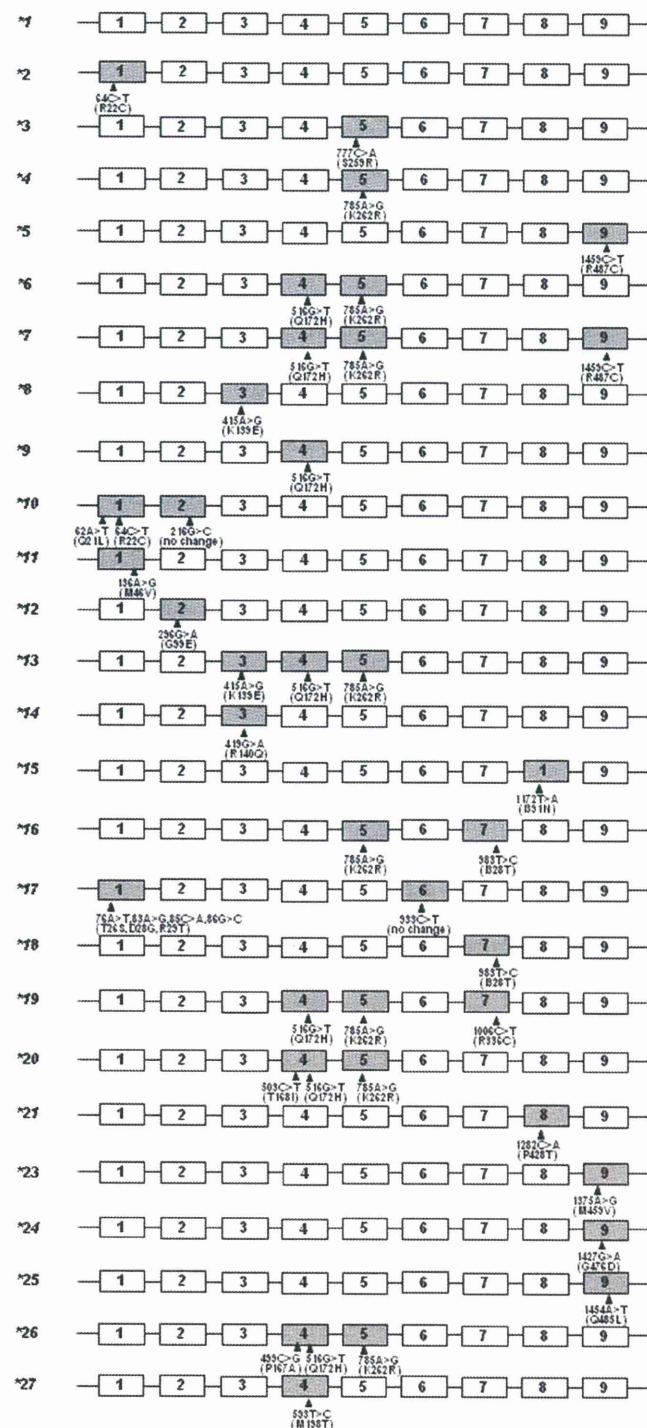


Fig. 2. Structures of *CYP2B6* alleles characterized in this study. The nine exons are indicated by numbered boxes. Some promoter and intronic polymorphisms are not shown.

added. The resulting mixture was vortexed. After centrifugation at 12,000g for 10 min, 80 μ l of the supernatant was transferred to a new plastic tube and passed through a filter (pore size: 0.2 μ m; YMC Co., Ltd., Kyoto, Japan). Subsequently, 10 μ l of the filtered solution was injected into the liquid chromatography-tandem mass spectrometry (LC-MS/MS) system for analysis. All peaks were integrated automatically by Xcalibur software (Thermo Fisher Scientific, Waltham, MA). Levels of DHA were calculated from the calibration curves by the ratios of their peak areas to that of ART. An eight-point calibration curve was plotted for DHA concentration (0.1, 0.2, 0.5, 1.0, 2.5, 5.0, 10, and 20 μ M).

Sample Preparation for Analysis of Specific Activity. AM demethylation activity was determined by measurement of the formation of DHA, according to the method of Asimus and Ashton (2009), with minor modifications. AM stock solution (50 mM) was prepared in $\text{CH}_3\text{CN}/\text{H}_2\text{O}$ [50:50 (v/v)], and a working solution (500 μ M) was prepared by dilution of the stock solution in potassium phosphate buffer, pH 7.4. The incubation mixture contained AM as a substrate (1 and 50 μ M), recombinant P450 enzymes (CYP1A1, CYP1A2, CYP1B1, CYP2A6, CYP2B6, CYP2C8, CYP2C9, CYP2C19, CYP2D6, CYP2E1, CYP2J2, CYP3A4, CYP3A5, and CYP4A11; 0.5 pmol) or human liver microsomes (50 μ g), 0.5 mM NADPH, 5 mM MgCl_2 , and 50 mM potassium phosphate buffer to a final volume of 90 μ l. After preincubation (3 min at 37°C), the reaction was started by addition of NADPH. Reactions were performed for 30 min and terminated by the addition of 100 μ l of methanol. Then, 5 μ l of internal standard (ART at 100 μ M) and 100 μ l of H_2O were added. The resulting mixture was vortexed. After centrifugation at 12,000g for 10 min, 80 μ l of the supernatant was transferred to a new plastic tube and passed through a filter (pore size: 0.2 μ m; YMC). Then, 10 μ l of the filtered solution was injected into the LC-MS/MS system for analysis. All peaks were integrated automatically by Xcalibur software. Levels of DHA were calculated from the calibration curves by using the ratios of their peak areas to that of ART. Formation of DHA was in the linear range between 10 and 60 min and 30 and 50 μ g of microsomal protein.

Sample Preparation for Analysis of Kinetic Parameters of CYP2B6 and CYP3A4. AM stock solution (50 mM) was prepared in $\text{CH}_3\text{CN}/\text{H}_2\text{O}$ [50:50 (v/v)], and working solutions (0.25, 0.50, 1.25, 2.5, 5.0, 12.5, and 25 mM) were prepared by dilution of the stock solution. These solutions were diluted with 50 mM potassium phosphate buffer, pH 7.4, and the final calibration curves were obtained with 0.5, 1.0, 2.5, 5.0, 10, 25, 50, and 100 μ M. CYP2B6 and CYP3A4 activity was evaluated using the concentration ranges 0.5 to 50 and 2.5 to 100 μ M, respectively. Samples were prepared as described above.

Determination of DHA and ART Using Online Column-Switching LC-MS/MS. Levels of DHA were determined by the LC-MS/MS method described by Huang et al. (2009), with minor modifications. A Nanospace S1-2 LC system, comprising an LC pump, autosampler, column oven maintained at 40°C, and on-line degasser (Shiseido, Tokyo, Japan), was used. The on-line column-switching valve system consisted of an automated switching valve (six-port valve) connected to pump A and pump B. Pump A was connected via the switching valve to the trap column, a CAPCELL PAK C18 SG II (10 \times 2 mm i.d., 3- μ m particle size) (Shiseido, Tokyo, Japan), and pump B was connected via the switching valve to the analytical column, a Sunfire C18 (150 mm \times 2.1 mm i.d., 3.5- μ m particle size) (Waters, Milford, MA). The outlet of

the analytical column was connected to the mass spectrometer via a divert valve.

Sample loading. A 10- μ l aliquot of sample was injected onto the trap column using pump B with the switching valve in position 1. Impurities on the trap column were eluted to waste using 0.1% $\text{HCOOH}-\text{H}_2\text{O}/\text{CH}_3\text{CN}$ [5:95 (v/v)] at a flow rate of 200 μ l/min for 4 min. Concurrently, initial flow was maintained by pump A at 200 μ l/min with 10 mM $\text{HCOONH}_4-\text{H}_2\text{O}$ (adjusted to pH 4.1 using HCOOH)-0.1% $\text{HCOOH}-\text{CH}_3\text{CN}$ [20:80 (v/v)] via the analytical column.

Sample elution. At 4 min, the switching valve was switched to position 2 to allow the purified DHA and ART to be eluted from the trap column onto the analytical column and subsequently into the mass spectrometer. Isocratic flow was maintained by pump B at a rate of 200 μ l/min for 11 min. Concurrently, the flow from pump A was passed through the trap column and diverted directly to waste. At 11 min, the switching valve was switched back to position 1, and the configuration of the online column switching system reverted back to that in the initial conditions (described for the sample loading above). A divert valve was used to divert the LC effluent to waste during the first 4.5 min and last 0.5 min of the chromatographic run. The total run time was 11 min.

Quantification analyses by MS were performed in the selected reaction monitoring mode because of the high selectivity and sensitivity of selected reaction monitoring data acquisition, in which the transitions of the precursor ion into the product ion were monitored: m/z 302 \rightarrow 145 and 302 \rightarrow 267 for DHA and m/z 300 \rightarrow 151 and 300 \rightarrow 209 for ART. The optimized parameters for MS are as follows: positive heated electrospray ionization voltage, 3 kV; heated capillary temperature, 300°C; sheath gas pressure, 50 psi; auxiliary gas setting, 20 psi; and heated vaporizer temperature, 300°C. Both the sheath and auxiliary gases were nitrogen. The collision gas was argon at a pressure of 1.5 mTorr. The LC-MS/MS system was controlled by Xcalibur software, and data were also collected with this software. The retention times of DHA and ART were 7.0 and 7.5 min, respectively.

Liver Specimens. Human liver specimens were obtained from the Human and Animal Bridging Research Organization (HAB) in Chiba, Japan, using frozen human livers (most of the donors were white). Microsomes were prepared from these specimens using differential centrifugation. Research protocols were approved by the ethics committees of the Graduate School of Pharmaceutical Sciences, Tohoku University (Sendai, Japan).

Expression of CYP2B6 Variant Proteins in COS-7 Cells. CYP2B6 variant proteins were expressed in COS-7 cells as described by Watanabe et al. (2010).

Determination of Protein Expression Levels by Immunoblotting. Western blotting was performed according to standard procedures, with 10% SDS-polyacrylamide gel electrophoresis, and 30- μ g microsomal fractions were loaded into each lane. Recombinant CYP2B6 Supersomes reagent (BD Gentest) was coanalyzed as the standard on each gel and used to quantify the CYP2B6 protein. The CYP2B6 protein was detected using the antihuman CYP2B6 antibody (BD Gentest) and horseradish peroxidase-conjugated goat anti-rabbit IgG (Dako Denmark A/S, Glostrup, Denmark). CYP3A4 Baculosomes reagent (Invitrogen) was coanalyzed as the standard on each gel and used to quantify the CYP3A4 protein. The CYP3A4 protein was detected using the antihuman CYP3A4 antibody (Nosan, Yokohama, Japan) and horseradish peroxidase-conjugated goat anti-rabbit IgG (Dako Denmark A/S). Immuno-

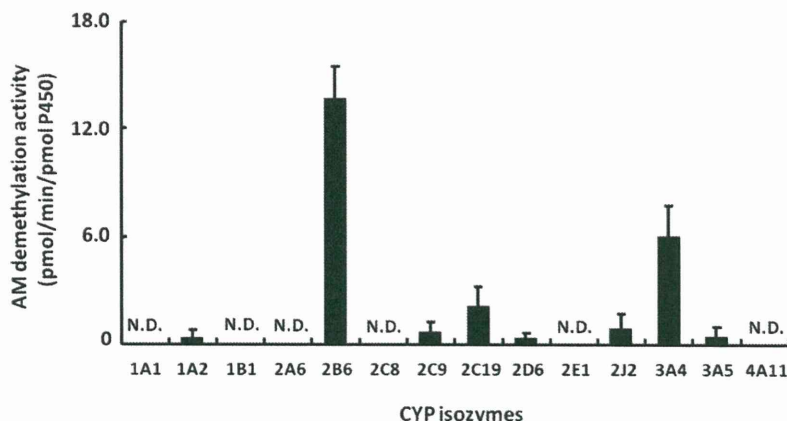


FIG. 3. AM demethylation activity of 14 P450 isozymes. The concentration of AM was 50 μ M. Each number corresponds to a P450 subtype. Results are presented as the mean \pm S.D. in triplicate. N.D., not detectable (activities were lower than 0.22 pmol \cdot min $^{-1}$ \cdot pmol P450 $^{-1}$).

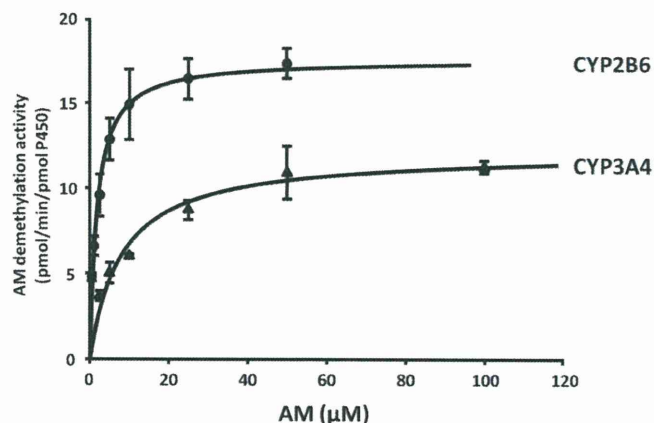


Fig. 4. The Michaelis-Menten curves for the demethylation of AM with recombinant CYP2B6 and CYP3A4.

blots were developed using the SuperSignal West Dura Extended Duration Substrate (Thermo Fisher Scientific). Chemiluminescence was quantified using a lumino-imaging analyzer (LAS-1000; FujiFilm, Tokyo, Japan) and ImageJ software (National Institutes of Health, Bethesda, MD).

Sample Preparation for Analysis of Kinetic Parameters of CYP2B6 Variants. Microsomal fractions (50 μg) obtained from COS-7 cells were used for evaluation of the activity of CYP2B6 variants. Samples were prepared as described above.

Statistical Analysis. Apparent K_m and V_{max} parameters were determined using nonlinear regression analysis. All data are the mean \pm S.D. in triplicate. Statistical analyses of enzymatic activities and kinetic parameters were performed by analysis of variance using the Dunnett method. $P \leq 0.05$ was considered significant.

Results

AM Demethylation by Recombinant Human P450s. The activities of AM demethylation were measured in 14 recombinant human P450 enzymes (CYP1A1, CYP1A2, CYP1B1, CYP2A6, CYP2B6, CYP2C8, CYP2C9, CYP2C19, CYP2D6, CYP2E1, CYP2J2, CYP3A4, CYP3A5, and CYP4A11) at 1 and 50 μM substrate concentrations. The lower concentration used was intended to approximate the plasma AM concentrations reported to be clinically relevant (0.3–1 μM) (Ali et al., 2010). At 1 μM AM, AM demethylation activities of recombinant CYP2B6 and CYP3A4 were 6.61 and 2.50 $\text{pmol} \cdot \text{min}^{-1} \cdot \text{pmol P450}^{-1}$, respectively. Under the lower substrate conditions used in this study, DHA was not formed by the other P450 isoforms with the exception of CYP2B6 and CYP3A4. At a higher concentration (50 μM), AM was principally metabolized by CYP2B6, followed by CYP3A4. A low rate of demethylation was observed for

CYP1A2, CYP2C9, CYP2C19, CYP2D6, CYP2J2, and CYP3A5; CYP1A1, CYP1B1, CYP2A6, CYP2C8, CYP2E1, and CYP4A11 were inactive (Fig. 3).

Kinetics of AM Demethylation by CYP2B6 and CYP3A4. The kinetics of AM demethylation were investigated for each of recombinant enzymes CYP2B6 and CYP3A4 by Michaelis-Menten plots (Fig. 4). Apparent K_m , V_{max} , and V_{max}/K_m values for CYP2B6 were estimated to be 1.95 μM , 17.9 $\text{pmol} \cdot \text{min}^{-1} \cdot \text{pmol P450}^{-1}$, and 9.19 $\mu\text{l} \cdot \text{min}^{-1} \cdot \text{pmol P450}^{-1}$, respectively; those for CYP3A4 were 8.24 μM , 12.3 $\text{pmol} \cdot \text{min}^{-1} \cdot \text{pmol P450}^{-1}$, and 1.49 $\mu\text{l} \cdot \text{min}^{-1} \cdot \text{pmol P450}^{-1}$, respectively, demonstrating a higher K_m and lower V_{max} , which resulted in an approximately one-sixth V_{max}/K_m value for CYP3A4 relative to that for CYP2B6.

Comparison of AM Demethylation Activities (at 50 μM AM) to Immunoquantified CYP2B6 and CYP3A4 Protein Levels in 13 Human Liver Microsomes. As shown in Fig. 5, AM demethylation activity in 13 human liver microsomes was correlated with immunoquantified CYP2B6 content ($r^2 = 0.548$, $P = 0.004$) but not with immunoquantified CYP3A4 content ($r^2 = 0.109$, $P = 0.272$).

Enzymatic Properties for AM Demethylation by Wild-Type and 25 Variant CYP2B6s. The demethylation activities of wild-type and 25 variant microsomal CYP2B6 proteins were determined using AM (50 μM) as a substrate (Fig. 6). For CYP2B6.8, CYP2B6.12, CYP2B6.18, CYP2B6.21, and CYP2B6.24, no AM demethylation activity was detected. The enzymatic activity of CYP2B6.3 could not be calculated because its expression level could not be determined by immunoblotting. CYP2B6.10, CYP2B6.11, CYP2B6.14, CYP2B6.15, CYP2B6.16, CYP2B6.20, and CYP2B6.27 exhibited significantly decreased activities compared with that of wild-type CYP2B6.

The Michaelis-Menten kinetics for AM demethylation were determined for CYP2B6.1, CYP2B6.2, CYP2B6.4, CYP2B6.5, CYP2B6.6, CYP2B6.7, CYP2B6.9, CYP2B6.10, CYP2B6.13, CYP2B6.14, CYP2B6.17, CYP2B6.19, CYP2B6.20, CYP2B6.23, CYP2B6.25, CYP2B6.26, and CYP2B6.27. The kinetic parameters are summarized in Table 1. The estimated kinetic parameters, apparent K_m , V_{max} , and $V_{max}/\text{apparent } K_m$ for AM demethylation by CYP2B6.1 were 3.10 μM , 36.0 $\text{pmol} \cdot \text{min}^{-1} \cdot \text{pmol CYP2B6}^{-1}$, and 12.4 $\mu\text{l} \cdot \text{min}^{-1} \cdot \text{pmol CYP2B6}^{-1}$, respectively. The V_{max} values for CYP2B6.14, CYP2B6.20, and CYP2B6.27 were significantly decreased, whereas those for CYP2B6.2, CYP2B6.4, and CYP2B6.6 were significantly increased, relative to that for the wild-type enzyme.

Discussion

In this study, we have determined the human P450 enzymes responsible for AM demethylation. Among 14 human P450s, CYP2B6

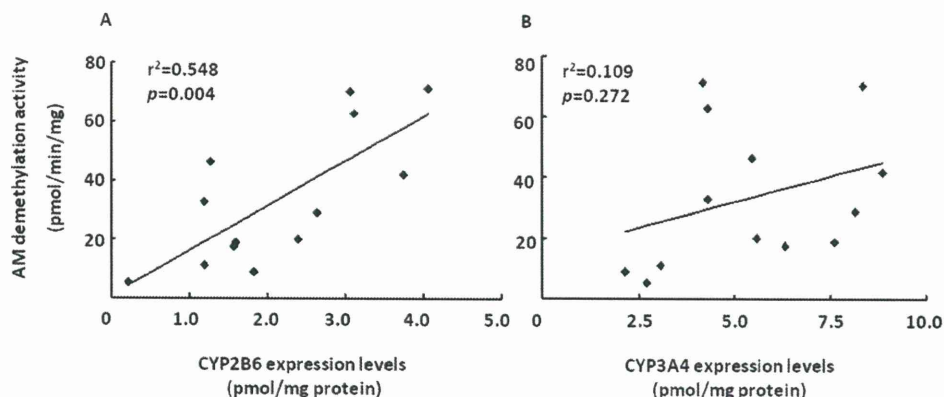


Fig. 5. Comparison of AM demethylation activities (at 50 μM AM) to immunoquantified CYP2B6 (A) and CYP3A4 (B) protein levels in 13 human liver microsomes. Correlation coefficients (r^2) obtained in these cases are shown.

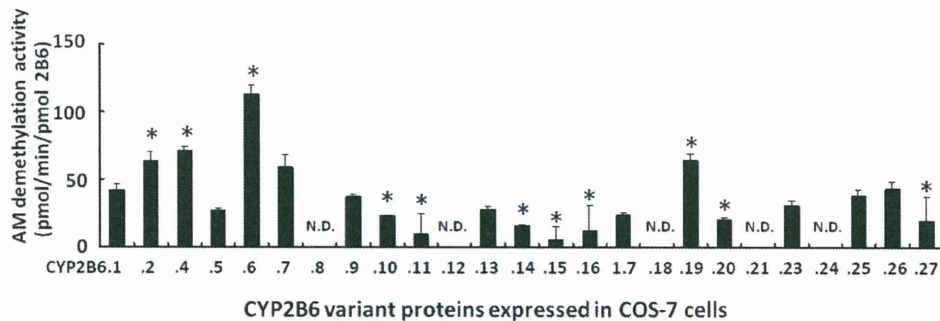


Fig. 6. AM demethylation activity of CYP2B6 proteins expressed in COS-7 cells. The concentration of AM was 50 μ M. Each number corresponds to CYP2B6 variant proteins. Results are presented as the mean \pm S.D. in triplicate. *, $P < 0.05$ compared with CYP2B6.1. N.D., not detectable.

has the highest intrinsic activity for AM demethylation, followed by CYP3A4. In the kinetic parameter analysis, the affinity of CYP2B6 was 4-fold higher than that of CYP3A4, and the $V_{max}/$ apparent K_m of CYP2B6 was 6-fold higher than that of CYP3A4. These results suggest that AM demethylation is likely to be mainly catalyzed by CYP2B6 in the liver. The contribution of CYP2B6 to AM demethylation by human liver microsomes was further substantiated by showing a correlation to CYP2B6 protein content ($r^2 = 0.548$). However, van Agtmael et al. (1999b,c) have reported that administration of AM with grapefruit juice, a CYP3A4 inhibitor, increased the blood concentration of AM and DHA but not their elimination half-life. Thus, CYP3A4 in the small intestine might also play an important role in the metabolism of AM.

CYP2B6 is a genetically polymorphic enzyme (Zanger et al., 2007; Arenaz et al., 2010). In vitro functional characterization of polymorphically expressed CYP2B6 variants revealed that CYP2B6.4 and CYP2B6.6 increased AM demethylation activity, whereas CYP2B6.8, CYP2B6.11, CYP2B6.12, CYP2B6.14, CYP2B6.15, CYP2B6.16, CYP2B6.18, CYP2B6.20, CYP2B6.21, CYP2B6.24, and CYP2B6.27 exhibited no activity or decreased activity. These alterations were consistent with those of previous in vitro studies performed using bupropion, 7-ethoxy-4-trifluoromethylcoumarin, and selegiline as CYP2B6 substrates (Lang et al., 2004; Klein et al., 2005; Wang et al., 2006; Rotger et al., 2007; Watanabe et al., 2010). However, CYP2B6.2 exhibited increased AM demethylation activity, and the activity of CYP2B6.13 was similar to that of wild-type CYP2B6.1. There have been several reports that CYP2B6.2 exhibited no functional differences compared with CYP2B6.1 (Jinno et al., 2003;

Watanabe et al., 2010) and that CYP2B6.13 had no metabolic activity toward 7-ethoxy-4-trifluoromethylcoumarin and selegiline (Watanabe et al., 2010). These results suggest that these CYP2B6 variants show substrate-dependent changes in the catalytic properties of the enzyme.

Gay et al. (2010) recently determined the crystal structure of CYP2B6, allowing the prediction of precise locations within the three-dimensional structure at which amino acid substitutions occur. They suggested that the K262R substitution on the G/H loop is assembled into a hydrogen-bonding network with His252, Thr255, Asp263, and Asp266 and is involved in protein stability. In this study, the AM demethylation activities of CYP2B6.12 (G99E) and CYP2B6.24 (Q476D) were not detectable. In the CYP2B6 protein structure, the Gly99 and Gln476 residues are located in substrate recognition site 1 and 6, respectively. These amino acid changes may reduce the affinity of CYP2B6 for AM. However, a number of amino acids with altered AM demethylation activity are located far from substrate recognition sites. Indeed, the apparent K_m values of AM demethylation were not significantly different among the CYP2B6 variants (Table 1). We hypothesize that the functional effects of these variants are transduced via long-range hydrogen-bonding networks or through subtle differences in the placement of secondary structural elements. In addition, most of the amino acid substitutions that abolished enzymatic activity are conserved among human P450s and are therefore critical for CYP2B6 activity.

This is the first study to functionally analyze CYP2B6 genetic variants with respect to AM demethylation activity. If CYP2B6 has a significant role in the metabolism of AM in vivo as well as in vitro, individuals with poor CYP2B6 metabolism might have higher plasma

TABLE 1

Kinetic parameters of AM demethylation by CYP2B6 proteins expressed in COS-7 cells

Results represent the mean \pm S.D. of triplicate determinations.

Variants	Apparent K_m μ M	V_{max} $pmol \cdot min^{-1} \cdot pmol \text{ CYP2B6}^{-1}$	$V_{max}/$ Apparent K_m $\mu l \cdot min^{-1} \cdot pmol \text{ CYP2B6}^{-1}$	$V_{max}/$ Apparent K_m Ratio % CYP2B6.1
CYP2B6.1	3.10 \pm 1.1	36.0 \pm 5.67	12.4 \pm 4.11	
CYP2B6.2	4.29 \pm 2.7	64.4 \pm 3.92*	18.8 \pm 9.19	129
CYP2B6.4	2.73 \pm 0.45	70.6 \pm 9.29*	26.0 \pm 2.42	223
CYP2B6.5	6.87 \pm 6.8	19.8 \pm 3.06	8.91 \pm 11.3	24.8
CYP2B6.6	6.72 \pm 3.0	150 \pm 15.9*	24.2 \pm 6.84	192
CYP2B6.7	2.80 \pm 1.4	50.1 \pm 12.3	19.2 \pm 4.65	154
CYP2B6.9	4.44 \pm 1.7	33.1 \pm 5.20	8.38 \pm 3.94	64.2
CYP2B6.10	1.93 \pm 0.68	17.0 \pm 5.03	9.98 \pm 5.05	75.7
CYP2B6.13	7.33 \pm 4.1	18.2 \pm 5.54	2.93 \pm 1.73	21.3
CYP2B6.14	5.06 \pm 5.8	7.06 \pm 1.63*	6.70 \pm 9.40	12.0
CYP2B6.17	2.17 \pm 0.40	21.2 \pm 4.73	9.44 \pm 2.45	84.0
CYP2B6.19	8.06 \pm 8.9	36.9 \pm 21.9	7.38 \pm 6.15	39.4
CYP2B6.20	6.47 \pm 9.8	9.85 \pm 2.22*	8.79 \pm 7.22	13.1
CYP2B6.23	1.91 \pm 0.72	31.4 \pm 7.71	17.6 \pm 5.93	142
CYP2B6.25	2.04 \pm 1.9	25.7 \pm 7.31	21.6 \pm 15.7	108
CYP2B6.26	5.50 \pm 3.4	37.3 \pm 6.04	10.1 \pm 8.13	58.4
CYP2B6.27	4.50 \pm 0.98	10.6 \pm 6.16*	2.59 \pm 1.82	20.2

* $P < 0.05$ compared with CYP2B6.1.

AM concentrations than those with more active variants of this enzyme. However, because DHA also has an antimalarial effect, it would be difficult to assess the clinical outcome in subjects who polymorphically express CYP2B6 without *in vivo* data. To more fully understand the mechanistic basis of our findings, it would be of great value to clinically examine the relationship between CYP2B6 genotypes and the plasma concentration of AM and its metabolites.

In conclusion, demethylation of AM was mainly catalyzed by recombinant CYP2B6, although recombinant CYP3A4 also exhibited this metabolic activity. In addition, we performed a comprehensive analysis, using COS-7 cells as a heterologous expression system, to characterize nonsynonymous CYP2B6 variants. Many of the 26 variants expressed in COS-7 cells exhibited significantly altered AM demethylation activity. This study provides insights into the genotype-phenotype associations of CYP2B6 and lays a foundation for future clinical studies on interindividual variation in drug efficacy and toxicity.

Authorship Contributions

Participated in research design: Honda, Hirasawa, and Hiratsuka.

Conducted experiments: Honda, Muroi, and Tamaki.

Contributed new reagents or analytic tools: Saigusa, Suzuki, Tomioka, and Matsubara.

Performed data analysis: Honda, Oda, and Hiratsuka.

Wrote or contributed to the writing of the manuscript: Honda, Saigusa, and Hiratsuka.

References

- Ali S, Najmi MH, Tarning J, and Lindegardh N (2010) Pharmacokinetics of artemether and dihydroartemisinin in healthy Pakistani male volunteers treated with artemether-lumefantrine. *Malar J* 9:275.
- Arenaz I, Vicente J, Fanlo A, Vázquez P, Medina JC, Conde B, González-Andrade F, and Sinués B (2010) Haplotype structure and allele frequencies of CYP2B6 in Spaniards and Central Americans. *Fundam Clin Pharmacol* 24:247–253.
- Asimus S and Ashton M (2009) Artemisinin—a possible CYP2B6 probe substrate? *Biopharm Drug Dispos* 30:265–275.
- Brewer TG, Grate SJ, Peggins JO, Weina PJ, Petras JM, Levine BS, Heiffer MH, and Schuster BG (1994) Fatal neurotoxicity of artemether and artemether. *Am J Trop Med Hyg* 51:251–259.
- Gautam A, Ahmed T, Batra V, and Paliwal J (2009) Pharmacokinetics and pharmacodynamics of endoperoxide antimalarials. *Curr Drug Metab* 10:289–306.
- Gay SC, Shah MB, Talakad JC, Maekawa K, Roberts AG, Wilderman PR, Sun L, Yang JY, Huelga SC, Hong WX, et al. (2010) Crystal structure of a cytochrome P450 2B6 genetic variant in complex with the inhibitor 4-(4-chlorophenyl)imidazole at 2.0-Å resolution. *Mol Pharmacol* 77:529–538.
- Hesse LM, Venkatakrishnan K, Court MH, von Moltke LL, Duan SX, Shader RI, and Greenblatt DJ (2000) CYP2B6 mediates the *in vitro* hydroxylation of bupropion: potential drug interactions with other antidepressants. *Drug Metab Dispos* 28:1176–1183.
- Hidestrand M, Oscarson M, Salonen JS, Nyman L, Pelkonen O, Turpeinen M, and Ingelman-Sundberg M (2001) CYP2B6 and CYP2C19 as the major enzymes responsible for the metabolism of selegiline, a drug used in the treatment of Parkinson's disease, as revealed from experiments with recombinant enzymes. *Drug Metab Dispos* 29:1480–1484.
- Hien TT and White NJ (1993) Qinghaosu. *Lancet* 341:603–608.
- Human Cytochrome P450 (CYP) Allele Nomenclature Committee (2008) CYP2B6 nomenclature. Available at: <http://www.cypalleles.ki.se/cyp2b6.htm>.
- Huang L, Jayewardene AL, Li X, Marzan F, Lizak PS, and Aweeka FT (2009) Development and validation of a high-performance liquid chromatography/tandem mass spectrometry method for the determination of artemether and its active metabolite dihydroartemisinin in human plasma. *J Pharm Biomed Anal* 50:959–965.
- Jinno H, Tanaka-Kagawa T, Ohno A, Makino Y, Matsushima E, Hanioka N, and Ando M (2003) Functional characterization of cytochrome P450 2B6 allelic variants. *Drug Metab Dispos* 31:398–403.
- Klayman DL (1985) Qinghaosu (artemisinin): an antimalarial drug from China. *Science* 228:1049–1055.
- Klein K, Lang T, Saussele T, Barbosa-Sicard E, Schunck WH, Eichelbaum M, Schwab M, and Zanger UM (2005) Genetic variability of CYP2B6 in populations of African and Asian origin: allele frequencies, novel functional variants, and possible implications for anti-HIV therapy with efavirenz. *Pharmacogenet Genomics* 15:861–873.
- Lang T, Klein K, Richter T, Zibat A, Kerb R, Eichelbaum M, Schwab M, and Zanger UM (2004) Multiple novel nonsynonymous CYP2B6 gene polymorphisms in Caucasians: demonstration of phenotypic null alleles. *J Pharmacol Exp Ther* 311:34–43.
- Le Bras J and Durand R (2003) The mechanisms of resistance to antimalarial drugs in *Plasmodium falciparum*. *Fundam Clin Pharmacol* 17:147–153.
- Lefèvre G, Carpentier P, Souppart C, Schmidli H, McClean M, and Stypinski D (2002) Pharmacokinetics and electrocardiographic pharmacodynamics of artemether-lumefantrine (Riamet) with concomitant administration of ketoconazole in healthy subjects. *Br J Clin Pharmacol* 54:485–492.
- Mo SL, Liu YH, Duan W, Wei MQ, Kanwar JR, and Zhou SF (2009) Substrate specificity, regulation, and polymorphism of human cytochrome P450 2B6. *Curr Drug Metab* 10:730–753.
- Mordi MN, Mansor SM, Navaratnam V, and Wernsdorfer WH (1997) Single dose pharmacokinetics of oral artemether in healthy Malaysian volunteers. *Br J Clin Pharmacol* 43:363–365.
- Mwesigwa J, Parikh S, McGee B, German P, Drysdale T, Kalyango JN, Clark TD, Dorsey G, Lindegardh N, Annerberg A, et al. (2010) Pharmacokinetics of artemether-lumefantrine and artesunate-amodiaquine in children in Kampala, Uganda. *Antimicrob Agents Chemother* 54:52–59.
- Na Bangchang K, Karbwang J, Thomas CG, Thanavibul A, Sukontason K, Ward SA, and Edwards G (1994) Pharmacokinetics of artemether after oral administration to healthy Thai males and patients with acute, uncomplicated falciparum malaria. *Br J Clin Pharmacol* 37:249–253.
- Nakajima M, Komagata S, Fujiki Y, Kanada Y, Ebi H, Itoh K, Mukai H, Yokoi T, and Minami H (2007) Genetic polymorphisms of CYP2B6 affect the pharmacokinetics/pharmacodynamics of cyclophosphamide in Japanese cancer patients. *Pharmacogenet Genomics* 17:431–445.
- Navaratnam V, Mansor SM, Sit NW, Grace J, Li Q, and Olliaro P (2000) Pharmacokinetics of artemisinin-type compounds. *Clin Pharmacokinet* 39:255–270.
- Price RN and Nosten F (2001) Drug resistant falciparum malaria: clinical consequences and strategies for prevention. *Drug Resist Updat* 4:187–196.
- Rotger M, Tegude H, Colombo S, Cavasini M, Furrer H, Décosterd L, Bliedernicht J, Saussele T, Günthard HF, Schwab M, et al. (2007) Predictive value of known and novel alleles of CYP2B6 for efavirenz plasma concentrations in HIV-infected individuals. *Clin Pharmacol Ther* 81:557–566.
- Roy P, Yu LJ, Crespi CL, and Waxman DJ (1999) Development of a substrate-activity based approach to identify the major human liver P-450 catalysis of cyclophosphamide and ifosfamide activation based on cDNA-expressed activities and liver microsomal P-450 profiles. *Drug Metab Dispos* 27:655–666.
- Salonen JS, Nyman L, Boobis AR, Edwards RJ, Watts P, Lake BG, Price RJ, Renwick AB, Gómez-Lechón MJ, Castell JV, et al. (2003) Comparative studies on the cytochrome p450-associated metabolism and interaction potential of selegiline between human liver-derived *in vitro* systems. *Drug Metab Dispos* 31:1093–1102.
- van Agtmael MA, Cheng-Qi S, Qing JX, Mull R, and van Bostel CJ (1999a) Multiple dose pharmacokinetics of artemether in Chinese patients with uncomplicated falciparum malaria. *Int J Antimicrob Agents* 12:151–158.
- van Agtmael MA, Gupta V, van der Graaf CA, and van Bostel CJ (1999b) The effect of grapefruit juice on the time-dependent decline of artemether plasma levels in healthy subjects. *Clin Pharmacol Ther* 66:408–414.
- van Agtmael MA, Gupta V, van der Wösten TH, Rutten JP, and van Bostel CJ (1999c) Grapefruit juice increases the bioavailability of artemether. *Eur J Clin Pharmacol* 55:405–410.
- van Agtmael MA, Van Der Graaf CA, Dien TK, Koopmans RP, and van Bostel CJ (1998) The contribution of the enzymes CYP2D6 and CYP2C19 in the demethylation of artemether in healthy subjects. *Eur J Drug Metab Pharmacokinet* 23:429–436.
- Wang J, Sönnnerborg A, Rane A, Josephson F, Lundgren S, Stähle L, and Ingelman-Sundberg M (2006) Identification of a novel specific CYP2B6 allele in Africans causing impaired metabolism of the HIV drug efavirenz. *Pharmacogenet Genomics* 16:191–198.
- Watanabe T, Sakuyama K, Sasaki T, Ishii Y, Ishikawa M, Hirasawa N, and Hiratsuka M (2010) Functional characterization of 26 CYP2B6 allelic variants (CYP2B6.2-CYP2B6.28, except CYP2B6.22). *Pharmacogenet Genomics* 20:459–462.
- Wernsdorfer WH (1991) The development and spread of drug-resistant malaria. *Parasitol Today* 7:297–303.
- Woodrow CJ, Haynes RK, and Krishna S (2005) *Artemisinin Postgrad Med J* 81:71–78.
- World Health Organization (2010) *Guidelines for Treatment of Malaria*, 2nd ed., World Health Organization, Geneva, Switzerland. Available from http://whqlibdoc.who.int/publications/2010/9789241547925_eng.pdf.
- Xie H, Griskevicius L, Stähle L, Hassan Z, Yasar U, Rane A, Broberg U, Kimby E, and Hassan M (2006) Pharmacogenetics of cyclophosphamide in patients with hematological malignancies. *Eur J Pharm Sci* 27:54–61.
- Xie HJ, Yasar U, Lundgren S, Griskevicius L, Terelius Y, Hassan M, and Rane A (2003) Role of polymorphic human CYP2B6 in cyclophosphamide bioactivation. *Pharmacogenomics J* 3:53–61.
- Zanger UM, Klein K, Saussele T, Bliedernicht J, Hofmann MH, and Schwab M (2007) Polymorphic CYP2B6: molecular mechanisms and emerging clinical significance. *Pharmacogenomics* 8:743–759.

Address correspondence to: Dr. Masahiro Hiratsuka, Laboratory of Pharmacotherapy of Life-Style Related Diseases, Graduate School of Pharmaceutical Sciences, Tohoku University, Sendai, Japan, 6-3, Aoba, Aramaki, Aoba-ku, Sendai 980-8578, Japan. E-mail: mhira@mt.hok.ac.jp

Selective inhibition of EGFR and VEGFR2 tyrosine kinases controlled by a boronic acid substituent on 4-anilinoquinazolines†

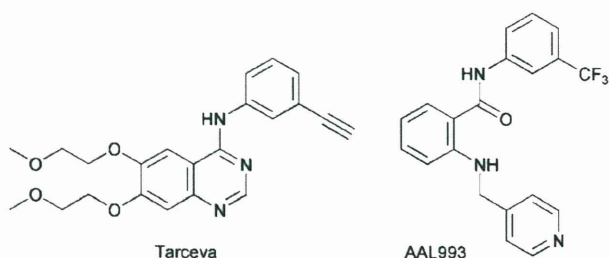
Hiroyuki Nakamura,* Ryoji Horikoshi, Taikou Usui and Hyun Seung Ban

Received 20th July 2010, Accepted 13th August 2010

DOI: 10.1039/c0md00115e

Boronic acid-containing 4-anilinoquinazolines were synthesized as selective inhibitors of EGFR and VEGFR2 tyrosine kinases. The substituted position of the boronic acid is essential for control of both kinase inhibitions, and the boronic acid substituted at the *para* position of the aniline moiety exhibited significant inhibition of VEGFR2 tyrosine kinase.

Growth factor receptor tyrosine kinases play an important role for the signal transduction pathway in cell proliferation. Deregulation of the signaling pathway has been observed in many human tumors, thus these kinases have been investigated as potential targets for cancer therapy.¹ The kinase inhibitors competitively bind to the ATP binding site of the protein kinases, which is relatively conserved, therefore enzymatic selectivity has been required for development of the kinase inhibitors. Among the various protein tyrosine kinase inhibitors reported,² the 4-anilinoquinazolines have proved to have great potential for selectivity and potency.³ In 1994, Fry and coworkers first found the 4-anilinoquinazoline (PD153035) to be a specific inhibitor of epidermal growth factor receptor (EGFR) tyrosine kinase.⁴ Based on their findings, ZD-1839 (Iressa™)^{5,6} and OSI-774 (Tarceva™)^{7,8} have been developed as EGFR tyrosine kinase inhibitors and approved for non-small cell lung cancer (NSCLC) therapy. In the meantime, various 4-anilinoquinazoline framework-based protein kinase inhibitors have been reported including cyclin-dependent kinase 2 (CDK2),⁹ Src and Abl kinases,¹⁰ vascular endothelial growth factor receptor (VEGFR) tyrosine kinases,¹¹ and platelet-derived growth factor receptor (PDGFR) kinase.¹²



Although organoborons have been developed as nucleophilic reagents for C–C bond formation in organic synthesis,¹³ the use of boron as a candidate functional group to interact with a target protein is an attractive strategy for drug design in medicine. A boron atom has a vacant orbital and interconverts with ease

between the neutral sp² and the anionic sp³ hybridization states, which generates a new stable interaction between a boron atom and a donor molecule through a covalent bond. In particular, several boronic acid compounds have been studied as enzyme inhibitors including thrombin,¹⁴ lactamases,¹⁵ dipeptidyl peptidases,¹⁶ and others.^{17–20} However, the most promising achievement in the area of boron pharmaceuticals is the development of bortezomib (PS341), a proteasome inhibitor,²¹ recently approved for clinical treatment of relapsed multiple myeloma and mantle cell lymphoma. The X-ray crystal structure of the 20S proteasome in complex with bortezomib was reported. In this structure, the boronic acid of bortezomib covalently interacts with the Thr-1 hydroxyl in the active site of the 20S proteasome, forming the hybridized borate.²² Recently, we reported the prolonged inhibitory activity of a boron-conjugated 4-anilinoquinazoline toward the EGFR tyrosine kinase. The quantum mechanical docking simulation revealed that the boronic acid moiety substituted at the 6 position of the quinazoline with a benzyl linker formed a covalent B–O bond with Asp800 in addition to hydrogen bonds with Asp800 and Cys797, which may cause the prolonged inhibition of the compound toward EGFR tyrosine kinase.²³ In this paper, we introduce a boronic acid, as an alternative candidate for a functional group, into the 4-anilinoquinazoline framework in pharmaceutical drug design and found that the selective inhibition of EGFR and VEGFR tyrosine kinases was controlled by a boronic acid substituent on 4-anilinoquinazolines (Fig. 1).

The synthesis of the diboron coupling precursors **3** and **5** is shown in Scheme 1. Substitution of 4-chloroquinazoline **1** with 3-chloroaniline and 3-chloro-4-fluoroaniline gave the corresponding 4-anilinoquinazolines **3a** and **3b** in 69 and 87% yields, respectively.²⁴ In a similar manner, 4-chloroquinazoline **2** was reacted with 3-chloroaniline and 3-chloro-4-fluoroaniline, and the resulting 4-anilinoquinazolines **4a** and **4b** were treated with aqueous ammonia followed by anhydrous trifluoromethane

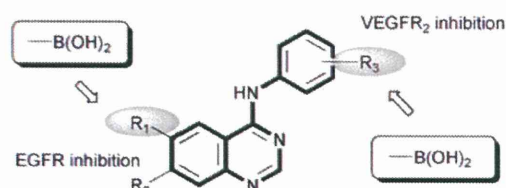
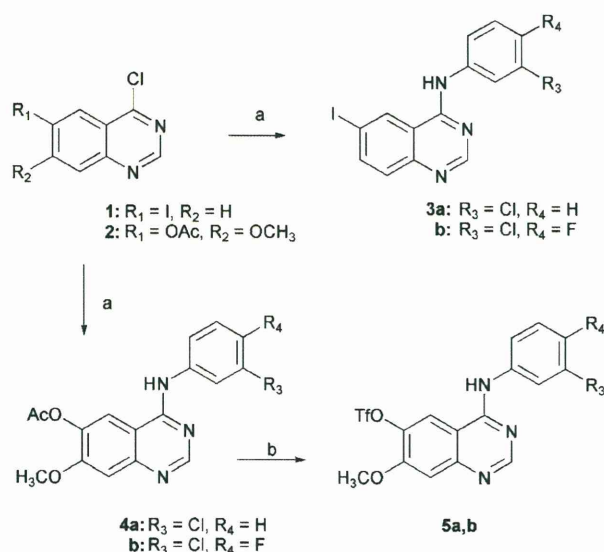


Fig. 1 Design of boronic acid-containing 4-anilinoquinazolines.

Department of Chemistry, Faculty of Science, Gakushuin University, Mejiro, Toshima-ku, Tokyo 171-8588, Japan. E-mail: hiroyuki.nakamura@gakushuin.ac.jp; Fax: +81 3 3986 0221; Tel: +81 3 5992 1029

† Electronic supplementary information (ESI) available: Experimental procedures and full characterisation for all new compounds. See DOI: 10.1039/c0md00115e

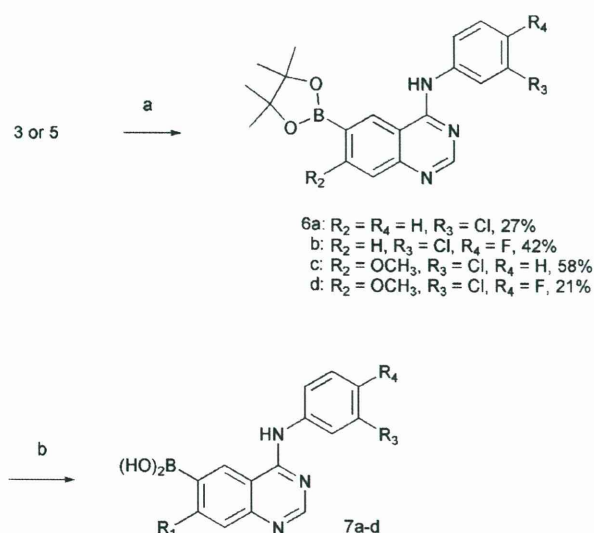


Scheme 1 Reagents and conditions: (a) anilines, isopropanol, reflux, **3a** (69%) or **3b** (87%); (b) i) 25% NH_3 aq; ii) Tf_2O , Py.

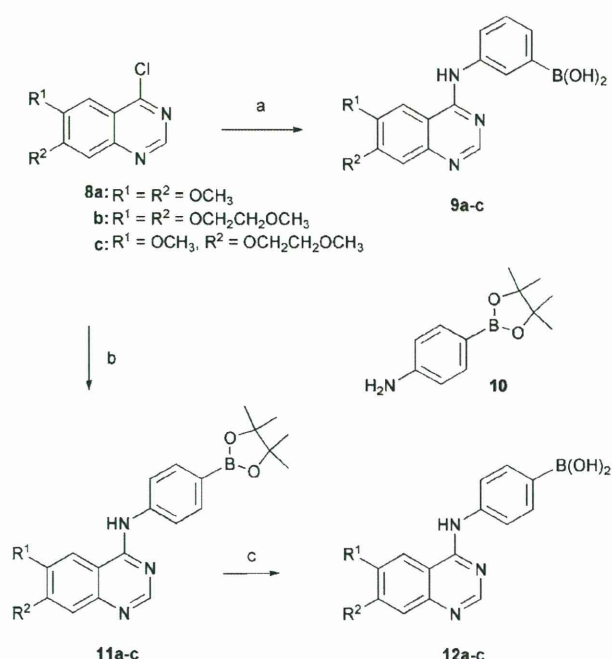
sulfonic acid to afford the corresponding triflates **5a** and **5b** in 15 and 66% yields, respectively, from **2** in three steps.

The Suzuki–Miyaura diboron coupling reaction was employed for **3** or **5** in the presence of palladium(II) catalysts in dimethylformamide (DMF) at 80 °C to give **6a–d** in 21–58% yields. Finally, deprotection of the pinacol boronate moiety was carried out under transesterification conditions using KHF_2 and phenylboronic acid to afford the corresponding boronic acids **7a–d** in 32–48% yields (Scheme 2).

Meanwhile, the boron-conjugated 4-anilinoquinazolines, in which a boronic acid moiety was substituted on the aniline ring, were synthesized by the substitution reaction of chloroquinazolines **8a–c** and boronated anilines as shown in Scheme 3. The



Scheme 2 Reagents and conditions: (a) pinacolatodiboron, PdCl_2 , dppf, KOAc, DMF, 80 °C; (b) i) KHF_2 , $\text{MeOH-H}_2\text{O}$; ii) PhB(OH)_2 .



Scheme 3 Reagents and conditions: (a) i) (3-aminophenyl)boronic acid, conc. HCl, isopropanol; ii) NaHCO_3 , $\text{MeOH-H}_2\text{O}$; (b) **10**, conc. HCl, isopropanol; (c) KHF_2 , $\text{MeOH-H}_2\text{O}$.

m-substituted boronic acids **9a–c** were obtained from **8a–c** with (3-aminophenyl)boronic acid under acidic conditions. On the contrary, the *p*-substituted boronic acids **12a–c** were obtained from **8a–c** with commercially available pinacolatoboronic ester **10** under acidic condition. The resulting boronic esters **11a–c** were treated with KHF_2 to afford the corresponding boronic acids **12a–c**.

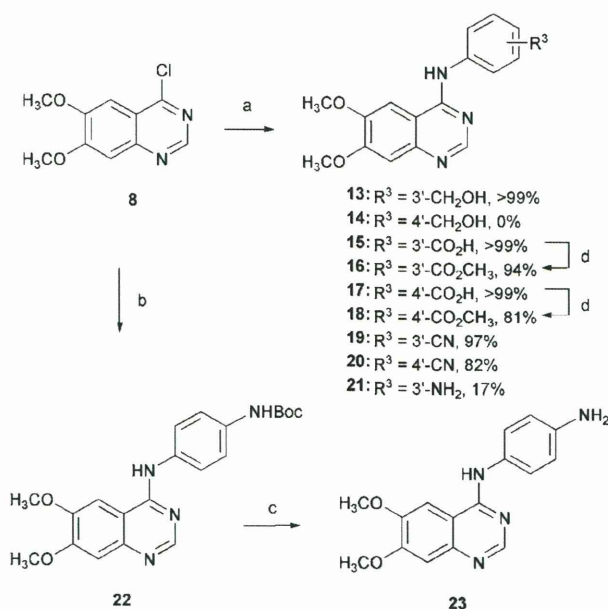
Inhibitory activity of the boron-conjugated 4-anilinoquinazolines **6**, **7**, **9** and **12** against EGFR, HER2, Flt-1 and KDR tyrosine kinases was determined by measuring the levels of phosphorylation of the tyrosine kinase-specific peptides (poly-(Glu:Tyr) substrate) *in vitro*.²⁵ As shown in Table 1, the boron-conjugated 4-anilinoquinazolines **6a–d** and **7a–d**, which have a boronate ester or boronic acid group substituted at the C-6 position of the quinazoline framework, selectively suppressed EGFR tyrosine kinase activity without inhibiting HER2, Flt-1 (VEGFR1 tyrosine kinase catalytic domain) or KDR (VEGFR2 tyrosine kinase catalytic domain) kinases, and their IC_{50} values against EGFR tyrosine kinase were at the range of 0.46–0.80 μM . On the contrary, the compounds **9a–c**, and **12a–c**, which have a boronic acid group substituted at the aniline ring of the quinazolines, displayed selective inhibition toward KDR tyrosine kinase. In particular, a boronic acid group substituted at the *para* position of the aniline, such as the compounds **12a–c**, is potent for significant inhibitory activity of KDR. The IC_{50} values of **12a** and **12b** are 0.036 and 0.037 μM , respectively, which is similar to that of a known KDR inhibitor, AAL993 ($\text{IC}_{50} = 0.014 \mu\text{M}$).²⁶

We next examined the effects of the boron-conjugated 4-anilinoquinazolines on the EGF-induced tyrosine phosphorylation of EGFR and the signaling cascades in A431 cells by immunoblot analysis. Treatment of A431 with EGF (10 ng ml^{-1}) rapidly

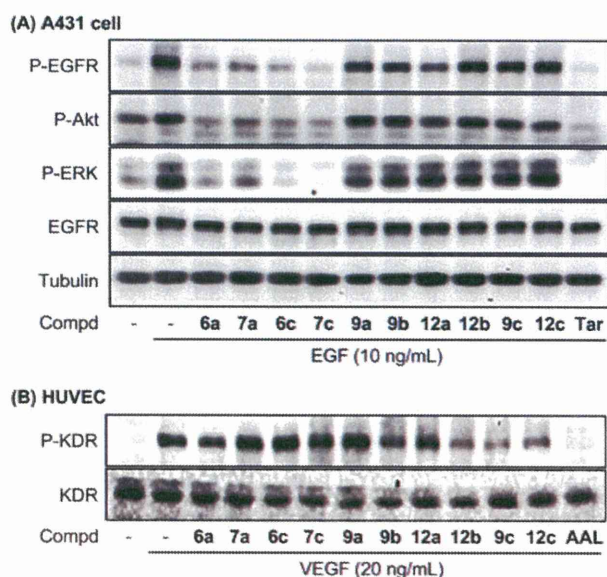
Table 1 Effect of the boron-conjugated 4-anilinoquinazolines on tyrosine kinase activity of EGFR, HER2, Flt-1, and KDR

Compds	IC ₅₀ /μM ^a			
	EGFR	HER2 ^b	Flt-1 ^b	KDR ^b
6a	0.59 ± 0.03	>1 (31)	>1 (12)	>1 (-)
6b	0.57 ± 0.04	>1 (-)	>1 (8)	>1 (-)
6c	0.49 ± 0.08	>1 (-)	>1 (-)	>1 (-)
6d	0.52 ± 0.07	>1 (-)	>1 (-)	>1 (-)
7a	0.65 ± 0.02	>1 (15)	>1 (7)	>1 (-)
7b	0.80 ± 0.07	>1 (-)	>1 (-)	>1 (-)
7c	0.46 ± 0.05	>1 (-)	>1 (-)	>1 (-)
7d	0.51 ± 0.01	>1 (-)	>1 (-)	>1 (-)
9a	>1 (46)	>1 (-)	>1 (-)	0.39 ± 0.03
9b	>1 (24)	>1 (-)	>1 (-)	0.19 ± 0.02
9c	>1 (45)	>1 (-)	>1 (19)	0.18 ± 0.02
12a	>1 (40)	>1 (-)	>1 (49)	0.036 ± 0.006
12b	>1 (36)	>1 (-)	>1 (41)	0.037 ± 0.012
12c	>1 (28)	>1 (-)	>1 (-)	0.86 ± 0.12
Tarceva	0.047 ± 0.003	>1 (-)	>1 (-)	>1 (38)
AAL993	>1 (30)	>1 (-)	>1 (-)	0.014 ± 0.002

^a The drug concentrations required to inhibit the phosphorylation of the poly(Glu:Tyr) substrate by 50% (IC₅₀) were determined from semilogarithmic dose-response plots, and results represent mean ± s.d. of triplicate samples. Percent of inhibition at 1 μM concentration was indicated in parentheses. ^b -, no inhibitory effect at 1 μM.

**Scheme 4** Reagents and conditions: (a) anilines, isopropanol, reflux; (b) 4-(BocNH)C₆H₄NH₂, isopropanol, reflux, 87%; (c) TFA, CH₂Cl₂, >99%; (d) conc. HCl, CH₃OH.

induced autophosphorylation of EGFR, and the level of the phosphorylation reached a maximum at 10 min after EGF stimulation. Under these conditions, the boron-conjugated 4-anilinoquinazolines, 6a-d and 7a-d, potently suppressed the EGF-induced phosphorylation of EGFR at 1 μM concentration

**Fig. 2** Inhibition of the EGF-induced phosphorylation of EGFR and VEGF-induced phosphorylation of KDR. (A) A431 cells were incubated with the boron-conjugated 4-anilinoquinazolines (1 μM) or Tarceva (0.3 μM) and then stimulated with EGF (10 ng mL⁻¹). (B) HUVECs were incubated with the boron-conjugated 4-anilinoquinazolines (1 μM) or AAL993 (1 μM) and then stimulated with VEGF (20 ng mL⁻¹). The levels of each kinase were detected by immunoblot analysis with the specific antibody.

of compounds, whereas compounds 9a-c and 12a-c did not affect the EGFR phosphorylation at this concentration (Fig. 2A). It has been reported that the autophosphorylation of EGFR tyrosine kinase activated various downstream kinases including ERK and Akt, which play an important role in the regulation of cell proliferation and apoptosis, respectively.²⁷ Therefore, we examined the effects on the EGFR-dependent activation of downstream signaling pathways. The boron-conjugated 4-anilinoquinazolines, 6a-d and 7a-d, also significantly suppressed the EGF-induced phosphorylation of ERK and Akt in parallel with the inhibition of EGFR autophosphorylation. However, these inhibitions were not observed in compounds 9a-c and 12a-c. These results indicate that the boron-conjugated 4-anilinoquinazolines, 6a-d and 7a-d, also induce the inhibitory effect on autophosphorylation of EGFR tyrosine kinase in cells as well as EGFR kinase *in vitro*, and arrest the downstream signaling pathway. Furthermore, we examined the effects of the boron-conjugated 4-anilinoquinazolines on the VEGF-induced phosphorylation of KDR in HUVECs. As shown in Fig. 2B, boron-conjugated 4-anilinoquinazolines 9b, 9c, 12b and 12c significantly suppressed VEGF-induced KDR phosphorylation. Although compounds 9a and 12a potently inhibited KDR kinase activity (Table 1), their inhibitory effect on KDR phosphorylation in HUVECs was not observed. The discrepancy of results between kinase assay and immunoblotting analysis might be induced by the weak membrane permeability property of dimethoxy groups in compounds 9a and 12a.

Since the substitution of a boronic acid group on the aniline ring has been observed to be essential for selective inhibition of KDR tyrosine kinase, we next synthesized various functional groups-substituted 4-anilinoquinazolines from 4-chloroquinazolinone 8 and anilines, and examined their effects on tyrosine kinase activity of EGFR, HER2, Flt-1, and KDR. As shown in

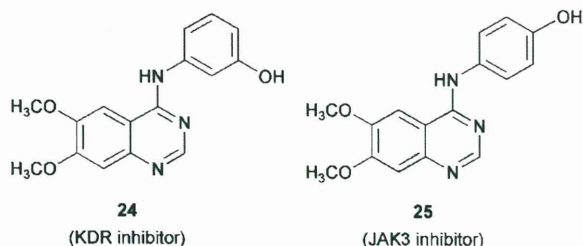
Table 2 Inhibition of the Various Functional Groups-Substituted 4-Anilinoquinazolines on Tyrosine Kinase Activity of EGFR, HER2, Flt-1, and KDR at 1 μM Concentration

Compds	% Inhibition at 1 μM ^a			
	EGFR ^b	HER2 ^b	Flt-1 ^b	KDR ^b
12a	40	—	49	99
12b	36	—	41	99
13	35	—	—	11
15	—	—	32	7
16	16	—	—	23
17	7	—	—	6
18	10	—	—	21
19	80	—	—	9
20	5	—	—	—
21	52	—	—	8
23	27	5	—	4
24	72	57	32	88
25	59	—	—	31
Tarceva	82	—	—	38
AAL993	30	—	34	95

^a Percent of inhibition of the phosphorylation of the poly(Glu:Tyr) substrate at 1 μM concentration was indicated. ^b —, no inhibitory effect at 1 μM .

Scheme 4, the substitution reaction proceeded and the corresponding 4-anilinoquinazolines **13** and **15–20** were obtained in high yields, except 4-(4'-hydroxymethylanilino)quinazoline **14** and 4-(3'-aminoanilino)quinazoline **21**. The compound **14** generated from **8** and 4-hydroxymethylaniline was gradually decomposed in air and the reaction of **8** with 1,4-diaminobenzene gave the corresponding 4-anilinoquinazoline **21** in only 17% yield. In the synthesis of 4-(4'-aminoanilino)quinazoline **23**, the first substitution reaction of **8** with Boc-protected 1,4-diaminobenzene was carried out and the resulting compound **22** was treated with trifluoromethanesulfonic acid (TFA) to give **23** in quantitative yield.

Table 2 shows the inhibition of a variety of functional groups substituted on the aniline moiety of 4-anilinoquinazolines, such as hydroxymethyl,²⁸ carboxylic acid, methyl ester, cyano, and amine groups, toward various tyrosine kinase activity. Interestingly, compound **19**, which has a cyano group substituted on a *meta* position of the aniline moiety, displayed high inhibition of EGFR tyrosine kinase (80%) similar to Tarceva (82%) at 1 μM concentration, indicating that both cyano and acetylene groups can be similarly bound to the kinase pocket. In all cases except AAL993, significant inhibition of KDR tyrosine kinase was not observed at 1 μM .



Since a boronic acid has been observed as an essential function for selective KDR kinase inhibition, we next examined whether

the boronic acids **9a–c** and **12a–c** are active species in the kinase assay. It has been reported that an aryl boronic acid is able to undergo oxidation with reactive oxygen species (ROS) in cells to be converted to phenols.²⁹ Furthermore, 4-(3'-hydroxyanilino)quinazoline **24**, which is considered as an oxidation product of the corresponding boronic acid **9a**, was reported as a selective KDR inhibitor ($\text{IC}_{50} = 0.05 \mu\text{M}$),³⁰ and 4-(4'-hydroxyanilino)quinazoline **25**, which may be generated from the corresponding boronic acid **12a** in a similar manner, was reported as a selective JAK3 inhibitor ($\text{IC}_{50} = 9.1 \mu\text{M}$).³¹ Therefore, we synthesized the *meta*-hydroxyl derivative **24** and the *para*-hydroxyl derivative **25** according to the literature procedures^{30,32} and examined the inhibition toward various tyrosine kinase activity. As shown in Table 2, the *meta*-hydroxyl derivative **24** exhibited inhibitory potency of broad-spectrum tyrosine kinases, whereas the *para*-hydroxyl derivative **25** did not display significant inhibitory activity toward these kinases at 1 μM concentration. These results indicate that a boronic acid substituted on the aniline ring of the 4-anilinoquinazoline framework is essential for the selective inhibition of KDR tyrosine kinase.

Conclusions

We developed boronic acid-containing 4-anilinoquinazolines as selective inhibitors of EGFR and VEGFR2 tyrosine kinases. The substituted position of a boronic acid is essential for control of both kinase inhibitions. Since a boron atom is not observed in the living body, we believe that the current findings are promising for the utility of the boron atom as an alternative element in pharmaceutical drug design.

Notes and references

- 1 P. Blume-Jensen and T. Hunter, *Nature*, 2001, **411**, 355–365.
- 2 A. Levitzki, *Acc. Chem. Res.*, 2003, **36**, 462–469.
- 3 R. A. LeMahieu, M. Carson, W. C. Nason, D. R. Parrish, A. F. Welton, H. W. Baruth and B. Yaremko, *J. Med. Chem.*, 1983, **26**, 420–425.
- 4 D. W. Fry, A. J. Kraker, A. McMichael, L. A. Ambroso, J. M. Nelson, W. R. Leopold, R. W. Connors and A. J. Bridges, *Science*, 1994, **265**, 1093–1095.
- 5 A. E. Wakeling, S. P. Guy, J. R. Woodburn, S. E. Ashton, B. J. Curry, A. J. Barker and K. H. Gibson, *Canc. Res.*, 2002, **62**, 5749–5754.
- 6 M. Fukuoka, S. Yano, G. Giaccone, T. Tamura, K. Nakagawa, J.-Y. Douillard, Y. Nishiwaki, J. Vansteenkiste, S. Kudoh, D. Rischin, R. Eek, T. Horai, K. Noda, I. Takata, E. Smit, S. Averbuch, A. Macleod, A. Feyereislova, R.-P. Dong and J. Baselga, *J. Clin. Oncol.*, 2003, **21**, 2237–2246.
- 7 J. D. Moyer, E. G. Barbacci, K. K. Iwata, L. Arnold, B. Boman, A. Cunningham, C. DiOrto, J. Doty, M. J. Morin, M. P. Moyer, M. Neveu, V. A. Pollack, L. R. Pustilnik, M. M. Reynolds, D. Sloan, A. Theleman and P. Miller, *Canc. Res.*, 1997, **57**, 4838–4848.
- 8 F. A. Shepherd, J. Rodrigues Pereira, T. Ciuleanu, E. H. Tan, V. Hirsh, S. Thongprasert, D. Campos, S. Maoleekoonpiroj, M. Smylie, R. Martins, M. van Kooten, M. Dediu, B. Findlay, D. Tu, D. Johnston, A. Bezjak, G. Clark, P. Santabarbara, L. Seymour and the National Cancer Institute of Canada Clinical Trials Group, *N. Engl. J. Med.*, 2005, **353**, 123–132.
- 9 L. Shewchuk, A. Hassell, B. Wisely, W. Rocque, W. Holmes, J. Veal and L. F. Kuyper, *J. Med. Chem.*, 2000, **43**, 133–138.
- 10 J. Hong-Yun, W. Jiang-Xue, Z. Xiao-Feng, C. Jie-Min, Y. Shi-Ping, Y. Hai-Jiao, T. Li, Z. Yi-Xin and H. Wenlin, *Leuk. Res.*, 2009, **33**, 1512–1519.

- 11 K. Kubo, T. Shimizu, S.-i. Ohya, H. Murooka, A. Iwai, K. Nakamura, K. Hasegawa, Y. Kobayashi, N. Takahashi, K. Takahashi, S. Kato, T. Izawa and T. Isoe, *J. Med. Chem.*, 2005, **48**, 1359–1366.
- 12 T. Furuta, T. Sakai, T. Senga, T. Osawa, K. Kubo, T. Shimizu, R. Suzuki, T. Yoshino, M. Endo and A. Miwa, *J. Med. Chem.*, 2006, **49**, 2186–2192.
- 13 N. Miyaura and A. Suzuki, *Chem. Rev.*, 1995, **95**, 2457–2483.
- 14 C. Kettner, L. Mersinger and R. Knabb, *J. Biol. Chem.*, 1990, **265**, 18289–18297.
- 15 S. Ness, R. Martin, A. M. Kindler, M. Paetzel, M. Gold, S. E. Jensen, J. B. Jones and N. C. J. Strynadka, *Biochemistry*, 2000, **39**, 5312–5321.
- 16 S. J. Coutts, T. A. Kelly, R. J. Snow, C. A. Kennedy, R. W. Barton, J. Adams, D. A. Krolkowski, D. M. Freeman, S. J. Campbell, J. F. Ksiazek and W. W. Bachovchin, *J. Med. Chem.*, 1996, **39**, 2087–2094.
- 17 K. A. Koehler and G. E. Lienhard, *Biochemistry*, 1971, **10**, 2477–2483.
- 18 W. Prusoff, T. S. Lin, A. Pivazy, A. S. Sun and E. Birks, *Pharmacol. Ther.*, 1993, **60**, 315–329.
- 19 N. Suzuki, T. Suzuki, Y. Ota, T. Nakano, M. Kurihara, H. Okuda, T. Yamori, H. Tsumoto, H. Nakagawa and N. Miyata, *J. Med. Chem.*, 2009, **52**, 2909–2922.
- 20 D. S. Matteson, *Med. Res. Rev.*, 2008, **28**, 233–246.
- 21 A. F. Kisselev and A. L. Goldberg, *Chem. Biol.*, 2001, **8**, 739–758.
- 22 M. Groll, C. R. Berkers, H. L. Ploegh and H. Ova, *Structure*, 2006, **14**, 451–456.
- 23 H. S. Ban, T. Usui, W. Nabeyama, H. Morita, K. Fukuzawa and H. Nakamura, *Org. Biomol. Chem.*, 2009, **7**, 4415–4427.
- 24 M. D. Gaul, Y. Guo, K. Affleck, G. S. Cockerill, T. M. Gilmer, R. J. Griffin, S. Guntrip, B. R. Keith, W. B. Knight, R. J. Mullin, D. M. Murray, D. W. Rusnak, K. Smith, S. Tadepalli, E. R. Wood and K. Lackey, *Bioorg. Med. Chem. Lett.*, 2003, **13**, 637–640.
- 25 E. G. Barbacci, L. R. Pustilnik, A. M. Rossi, E. Emerson, P. E. Miller, B. P. Boscoe, E. D. Cox, K. K. Iwata, J. P. Jani, K. Provoncha, J. C. Kath, Z. Liu and J. D. Moyer, *Canc. Res.*, 2003, **63**, 4450–4459.
- 26 P. W. Manley, P. Furet, G. Bold, J. Bruggen, J. Mestan, T. Meyer, C. R. Schnell, J. Wood, M. Haberey, A. Huth, M. Kruger, A. Menrad, E. Ottow, D. Seidelmann, G. Siemeister and K. H. Thierach, *J. Med. Chem.*, 2002, **45**, 5687–5693.
- 27 J. S. Sebolt-Leopold and J. M. English, *Nature*, 2006, **441**, 457–462.
- 28 A. J. Barker, K. H. Gibson, W. Grundy, A. A. Godfrey, J. J. Barlow, M. P. Healy, J. R. Woodburn, S. E. Ashton, B. J. Curry, L. Scarlett, L. Henthorn and L. Richards, *Bioorg. Med. Chem. Lett.*, 2001, **11**, 1911–1914.
- 29 M. C. Y. Chang, A. Pralle, E. Y. Isacoff and C. J. Chang, *J. Am. Chem. Soc.*, 2004, **126**, 15392–15393.
- 30 L. F. Hennequin, A. P. Thomas, C. Johnstone, E. S. E. Stokes, P. A. Ple, J.-J. M. Lohmann, D. J. Ogilvie, M. Dukes, S. R. Wedge, J. O. Curwen, J. Kendrew and C. Lambert-van der Brempt, *J. Med. Chem.*, 1999, **42**, 5369–5389.
- 31 E. A. Sudbeck, X.-P. Liu, R. K. Narla, S. Mahajan, S. Ghosh, C. Mao and F. M. Uckun, *Clin. Canc. Res.*, 1999, **5**, 1569–1582.
- 32 G. W. Rewcastle, W. A. Denny, A. J. Bridges, H. Zhou, D. R. Cody, A. McMichael and D. W. Fry, *J. Med. Chem.*, 1995, **38**, 3482–3487.

Amphiphilic allylation of arylidene-1,3-oxazol-5(4H)-one using bis- π -allylpalladium complexes: an approach to synthesis of cyclohexyl and cyclohexenyl α -amino acids†

Afaf R. Genady^a and Hiroyuki Nakamura^{*b}

Received 13th June 2011, Accepted 7th July 2011

DOI: 10.1039/c1ob05952a

An efficient method for synthesis of cyclohexyl and cyclohexenyl α -amino acids *via* palladium-catalyzed three-component assemblies followed by ring-closing metathesis (RCM) is described. The present catalytic reaction is successfully extended to substituted benzylidene azlactones **2a–j** RCH=(1,3-oxazole): R = alkyl or aryl. The amphiphilic bis-allylation of these substrates has been achieved by replacing toxic allylstannanes with allyltrifluoroborate and the reaction proceeded smoothly to afford the corresponding 1,7-diene derivatives **3a–j** in acceptable to good yields. RCM of the resulting octadienes using the first generation Grubbs catalyst gave easy access to stereodefined substituted cyclohexene derivatives **7–11** in high yields. Acid hydrolysis of the oxazolone ring of **7–10** gave protected amino acids **12–16**. Debenzoylation of **13** and **15** afforded 1-amino-6-aryl-cyclohex-3-enecarboxylic acids **17** and **18** in excellent yields, respectively. Moreover, catalytic reduction of **13** gave the corresponding cyclohexane derivative **19** which could be debenzoylated to give 1-amino-2-phenylcyclohexene-1-carboxylic acid (**20**). The structures of compounds **9**, **12** and **13** were confirmed by X-ray structural analysis. It is an excellent method for creating a wide range of cyclic α,α -disubstituted α -amino acids.

Introduction

Transition metal-catalyzed multicomponent assembling reactions provide an efficient route for the construction of complex organic molecules.¹ Catalytic transformations involving nucleophilic attack on (η^3 -allyl)palladium intermediates have been widely applied in a number of important chemical processes,^{2–7} including allylic substitution and the oxidation of alkenes and conjugated dienes. Palladium-catalyzed allylation with various nucleophiles (Tsuji–Trost-type reaction) is now a very important modern organic transformation for the construction of carbon–carbon or carbon–heteroatom bonds.⁸ Furthermore, it has been demonstrated that, under catalytic conditions, bis- π -allylpalladium complexes can undergo an initial electrophilic attack on one of the allyl moieties followed by a nucleophilic attack on the other.^{9–14} This bis- π -allylpalladium complex can act as an amphiphilic reagent reacting with activated olefins and arynes to form the corresponding

bis-allylation products. Subsequently, several modifications of this reaction with variation of allyl sources, activated alkenes and catalysts have been reported by different groups.^{15,16} This catalytic amphiphilic bis-allylation could also be applied to the synthesis of medium-sized carbocycles.¹⁷ Moreover, regioselective unsymmetrical tetra-allylation of C₆₀ was reported recently using the catalytic amphiphilic bis-allylation reaction.¹⁸

In the past decade, organotrifluoroborates have become important reagents in organoboronate chemistry, in particular for transition-metal-catalyzed coupling reactions.^{16,19,20} These reagents are air- and thermostable species, which are usually easy to handle and purify. Moreover, allyltrifluoroborates have been shown to be effective allylating reagents for aldehydes.²² Recently, Batey and co-workers^{21,22} described the synthesis of a new class of allylboron compounds containing a trifluoroborate functionality. Due to the toxicity as well as the byproducts of organostannanes, we preferred the use of allyltrifluoroborate in catalytic bis- π -allylpalladium reactions. On the other hand, azlactones are important synthons for the synthesis of several biologically active compounds.²³ They are also particularly useful precursors for the synthesis of amino acids,²⁴ peptides,²⁵ heterocycles,²⁶ biosensors,²⁷ and antitumor²⁸ or anticancer²⁹ compounds.

The construction of suitably functionalized cyclohexene frameworks plays a central role in many natural product syntheses.³⁰ Although the Diels–Alder reaction is among the most powerful tools for generating such carbocycles,³¹ it is often difficult to form

^aDepartment of Chemistry, Faculty of Science, University of Tanta, 31527-Tanta, Egypt. E-mail: genadyafaf@yahoo.com

^bDepartment of Chemistry, Faculty of Science, Gakushuin University, 1-5-1 Mejiro, Toshima-ku, Tokyo 171-8588, Japan. E-mail: hiroyuki.nakamura@gakushuin.ac.jp; Fax: +81-3-5992-1029

† Electronic supplementary information (ESI) available: ¹H and ¹³C NMR spectra of compounds **3a–j** and **7–20**, and X-ray crystallographic files for compounds **9**, **12** and **13**. CCDC reference numbers 82954–82956. For ESI and crystallographic data in CIF or other electronic format see DOI: 10.1039/c1ob05952a

systems that are highly congested or possess substituent arrays that are incompatible with the reaction.³² A number of alternative methods for synthesizing cyclohexenes have arisen from catalytic approaches, such as the phosphine-catalyzed Rauhut–Currier reaction,³³ transition-metal-catalyzed ring-closing metathesis (RCM),³⁴ and cycloisomerization reactions.³⁵ In contradistinction to the widespread use of these intramolecular processes, intermolecular counterparts for catalytic cyclohexene synthesis are less well developed.^{36,37} With the development of air-stable, functionally compatible, and highly active ruthenium catalysts, such as the first-generation Grubbs catalyst³⁸ and second-generation Grubbs catalyst,³⁹ the ring-closing metathesis (RCM) reaction has become one of the most powerful methods to synthesize many kinds of cyclized products from acyclic diene or enyne precursors.⁴⁰ In this study, the first-generation Grubbs catalyst was used in the metathesis reaction of the resulting bis-allylated azlactones giving the corresponding cyclohexenes in excellent yields.

α,α -Disubstituted α -amino acids are nonproteinogenic modified amino acids, in which the hydrogen atom at the α -position of natural α -amino acids is replaced with an alkyl substituent.⁴¹ The α -alkyl substituents in α,α -disubstituted amino acids severely restrict the conformational freedom of peptides containing such residues, and these amino acids are used as a probe to investigate the biologically active conformation,⁴² to study the secondary structure of peptides,⁴³ and to search for the origin of chirality.⁴⁴ Furthermore, α,α -disubstituted α -amino acids are also found in many biologically active compounds, including antibiotics such as altemicidin.⁴⁵ Certain cyclic α,α -disubstituted amino acids, notably those with 3-, 5-, and 6-membered rings, tend to induce α -helical conformations when incorporated into peptides.⁴⁶ One of the challenges is to have procedures that provide flexible and simple methods for obtaining optically active α,α -disubstituted α -amino acids and that, furthermore, give diversity in structural and electronic properties.

Here we demonstrate a new protocol in amino acids synthesis; bis-allylated azlactones can act as excellent precursors for the synthesis of cyclic amino acids by bis-allylation of unsaturated azlactones. To the best of our knowledge, this is the first bis-allylation of azlactones. Catalytic cyclization of the resulting 1,7-diene afforded cyclohexene–azlactone adducts.

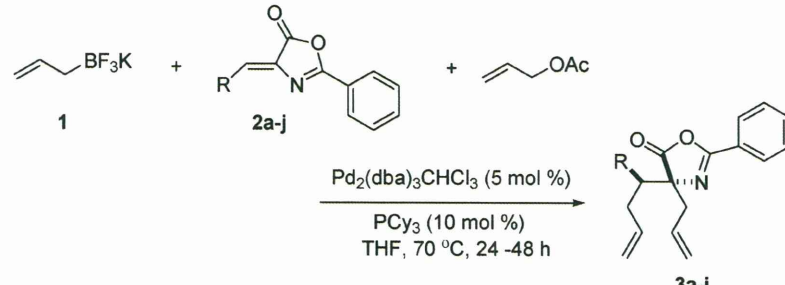
Results and discussion

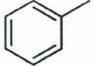
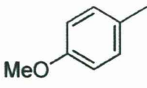
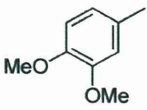
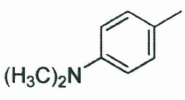
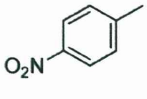

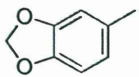
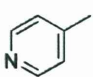
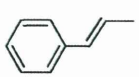
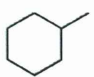
Catalytic amphiphilic bis-allylation

The three-component assembling reactions such as bis-allylation gave the corresponding α,β -functionalized products in high yields. Although these reactions are limited to highly activated olefins,¹⁶ we succeeded in utilizing substituted azlactones **2a–j** as substrates. In the current study, we used an alternative catalytic system of bis- π -allylpalladium complexes generated from allyltrifluoroborate (**1**). Arylidene azlactones **2a–g** and **2i** were prepared according to the classic Erlenmeyer synthesis,⁴⁷ whereas **2h** and alkylidene azlactone **2j** were prepared under mild conditions using alumina as a catalyst.⁴⁸ In a preliminary study,⁴⁹ we reported suitable conditions for the amphiphilic bis-allylation of arylidene malonitrile with allyl acetate and allyltrifluoroborate to give substituted 1,7-diene derivatives. The results prompted us to extend this methodology into other olefins such as arylidene

azlactones in bis-allylation reactions as a masked amino acid fragment. Moreover, we examined the optimization of palladium catalysts and ligands for amphiphilic bis-allylation of activated alkenes by replacing allylstannanes with allyltrifluoroborate.⁴⁹ According to these results we found that the amphiphilic bis-allylation reaction with allyltrifluoroborate and allyl acetate proceeded smoothly using $\text{Pd}_2(\text{dba})_3\text{CHCl}_3$ /tricyclohexylphosphine (PCy_3) in THF. These reaction conditions could be applied to azlactones **2**. The reaction of benzylidene azlactone **2a** (1 equiv.), allyltrifluoroborate **1** (1.5 equiv.), and allyl acetate (1.5 equiv.) in THF proceeded in the presence of $\text{Pd}_2(\text{dba})_3\text{CHCl}_3$ (5 mol%) and PCy_3 (10 mol%) in an argon atmosphere at 70 °C for 24 h to furnish 1,7-diene derivative **3a** in 45% yield. The low yield of **3a** could be explained by the formation of mono-allylated byproduct which was identified by ESI mass spectrometry. Increasing the reaction time had no effect on the bis-allylated yield. Moreover, allyl acetate gave the highest yield of three-component assembling product. Other substrates such as allyl chloride, which was considered the most appropriate for the amphiphilic bis-allylation with allyltributylstannane, were less effective for the reaction, affording **3a** in lower yield (26%). So, in another attempt to enhance the yield of the bis-allylated product, we performed the bis-allylation reaction using 3 equiv. of allyl acetate. It was found that the yield of **3a** increased to 49% (Table 1, entry 1). To study the scope of the reaction, attempting to enhance the activity of the double bond in azlactone, we used different aryl derivatives of azlactones. Several diversely substituted benzylidene azlactones underwent bis-allylation by this procedure to produce the corresponding 1,7-octadiene derivatives. The results are summarized in Table 1. This procedure is compatible with a wide range of substituents including electron donating and electron withdrawing groups substituted on the phenyl ring. Various substituted aryloxyidene azlactones **2b–i** underwent bis-allylation with **1** and allyl acetate to give the corresponding three-component assembling products **3b–3i** in good yields (entries 2–9).

Aryloxyidene azlactones with electron donating groups (entries 2–4) are more effective substrates for the assembling reaction than that bearing an electron withdrawing group on the phenyl ring (entry 5). The lower yield of **3d** compared to the yields of **3b** and **3c** was attributed to the insolubility of **2d** in THF and using DMF as the solvent (entry 4). The present protocol is successfully extended to azlactones with a heterocyclic substituent, such as furyl and pyridyl groups. Thus, treatment of furylidene azlactone (**2f**) and pyridylidene azlactone (**2h**) with **1** as well as allyl acetate in the presence of $\text{Pd}_2(\text{dba})_3\text{CHCl}_3/\text{PCy}_3$ afforded the corresponding 1,7-diene derivatives **3f** and **3h** in 73% and 62% yields, respectively (entries 6 and 8). Under similar conditions, the reaction of piperonylidene azlactone (**2g**) with **1** and allyl acetate produced the corresponding assembling product **3g** in 75% yield (entry 7). The bis-allylation reaction also proceeded with *E/Z*-cinnamylidene azlactone **2i** to give (*E/Z*)-4-allyl-2-phenyl-4-(1-phenylhexa-1,5-dien-3-yl)oxazol-5(4*H*)-one (**3i**) in 32% yield (entry 9). It should be noted that the allylation reaction is completely regioselective, adding to the β and α carbons of **2i**. No other regioisomer was detected as evidenced by the ¹H NMR spectrum of the crude reaction mixture, indicating that the catalytic allylation is highly regioselective. The three-component assembling reaction of alkylidene azlactone **2j** gave **3j** in 68% yield (entry 10). The purification of the bis-allylation product was

Table 1 Palladium-catalyzed double allylation of olefins **2a–j** with allyltrifluoroborate **1** and allyl acetate


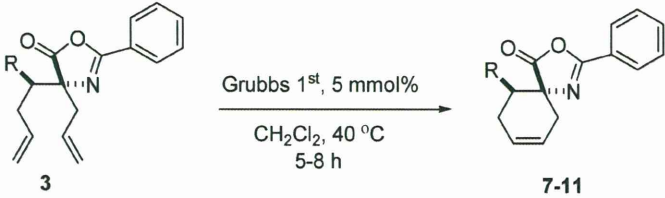
Entry	R	Product	Time (h)	Yield (%) ^a	d.r. ^b
1		3a	24	45	5:1
2		3b	24	58	4:1
3		3c	48	67	3:1
4		3d^c	24	47	3:1
5		3e	48	49	4:1
6		3f^e	24	73	5:1
7		3g	24	75	4:1
8		3h	24	62	3:1
9		3i	48	32	—
10		3j	24	68	4:1

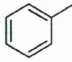
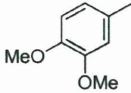

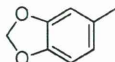
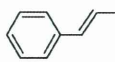
^a Combined isolated yields of two diastereomers based on **2**. ^b Diastereomer ratio determined by ¹H NMR. ^c DMF was used as the solvent.

performed by preparative thin layer chromatography (TLC) using hexane/ethyl acetate as the mobile phase. Diastereoselectivity (3–5:1) of the bis-allylation reactions was observed in all substituted azlactones **2a–j** except **2i** (Table 1). The major diastereomers were isolated by preparative TLC and identified.

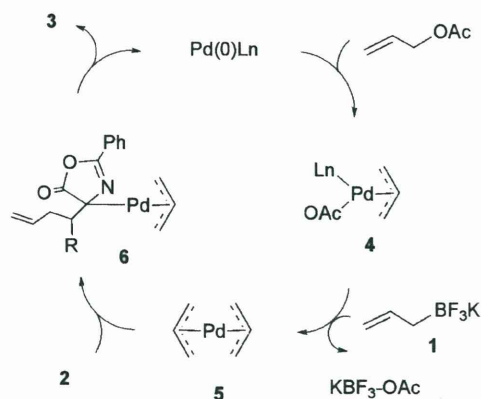
The proposed mechanism for the reaction course of this transformation is summarized in Scheme 1. On the basis of the known palladium chemistry and the mechanisms for the

catalytic reactions involving bis- π -allylpalladium complexes as key intermediates,^{9,17,50–52} a mechanism is proposed to account for the present catalytic amphiphilic bis-allylation reaction. The first step likely involves the oxidative addition of allyl acetate to Pd(0) to give π -allylpalladium acetate **4**. Transmetalation of allyltrifluoroborate **1** to π -allylpalladium acetate **4** gives bis- π -allylpalladium intermediate **5** and KBF₃OAc. Reaction of olefin **2** with **5** gives the complex **6**, which undergoes reductive elimination

Table 2 Metathesis reaction of **3**


Entry	3	Product	R	Yield (%) ^a
1	a 3	7		85
2	c 3	8		87
3	f 3	9		92
4	g 3	10		76
5	i 3	11		70

^a Isolated yields based on **3**.



Scheme 1 Palladium-catalysis mechanism.

to afford the corresponding bis-allylated product **3** and regenerate the Pd(0) catalyst.

Metathesis of bis-allylated compounds

Catalytic olefin metathesis transformed some of these bis-allylated products (**3a**, **3c**, **3f**, **3g** and **3i**) to the corresponding cyclohexenes (**7–11**) in 70–92% yields (Table 2).

In our experiments the metathesis of bis-allylated products to cyclohexenes worked with excellent results when the reaction was carried out in dichloromethane at reflux for 5–8 h in the presence of 1st generation Grubbs' catalyst, allowing the formation of the corresponding cyclohexenes. The metathesis of **3i** is highly

chemoselective giving the cinnamyl-substituted product **11**, exclusively (entry 5). The ¹H NMR spectrum of compound **11** showed δ - and γ -CH protons resonate at 5.9 and 6.5 ppm, respectively. It was possible to obtain X-ray quality crystals from **9** by slow evaporation of a CH₂Cl₂/hexane solution at room temperature. The solid state structure of the cyclohexene **9**, determined by X-ray diffraction, is depicted in Fig. 1. The cyclohexene **9** consists of a cyclohexene ring having azlactone and furan moieties as substituents at positions 1 and 6. The C–C bond lengths of the cyclohexene ring span over a narrow range of 1.495(2)–1.555(2) Å compared with the C=C bond distance 1.322(2) Å.

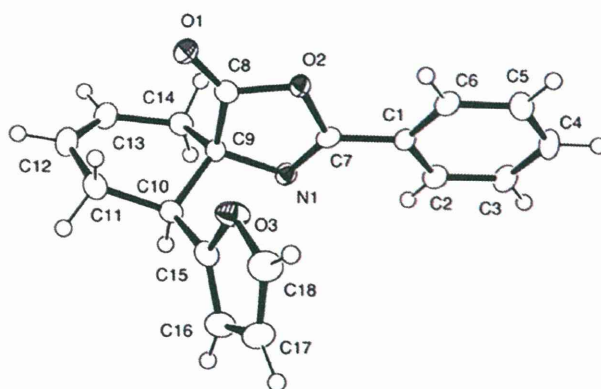
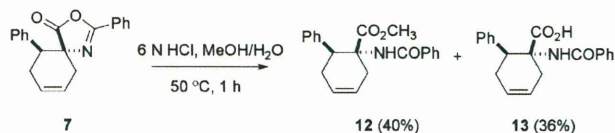


Fig. 1 ORTEP representation of **9**, showing 50% probability thermal ellipsoids.

Hydrolysis of oxazolone ring

One of the goals of our synthetic work was the successful preparation and characterization of a structurally diverse series of α,α -disubstituted α -amino acids derived from compounds 7–11. Incubation of azlactone 7 in a mixture of MeOH/H₂O (1 : 1) and HCl (6 N) at room temperature for 1 h resulted in cleavage of the oxazolone ring to give a mixture of 12 and 13 which could be isolated by preparative TLC to give 40% and 36% yields, respectively (Scheme 2).



Scheme 2 Cleavage of azlactone 7.

In the ¹H NMR spectra of 12 and 13, the new signals at 6.8 and 6.7 ppm indicated the presence of an NH group. ¹³C NMR spectra showed a low field shift of C=N of the former oxazolone ring in compounds 7–11, from *ca.* 160.2 ppm to *ca.* 166.8 ppm, whereas a high field shift of *ca.* 7 ppm for the carbonyl carbon of compounds 12 and 13 (172.8 ppm) compared with compound 7 (180.3 ppm) was observed. The expected deviations in these positions were attributed to oxazolone ring opening. Alternative conditions using a mixture of THF/aq. HCl (6 N) for direct conversion of 7 to the corresponding free carboxylic compound (13) were also possible. The compounds 12 and 13 crystallize in the monoclinic space groups *P*2₁/*c* and *C*2/*c*, respectively (Fig. 2, Table 3).

Similarly, compounds 8–10 were hydrolysed producing benzoylated amino acids 14–16 (Scheme 3). The structures of these compounds were also confirmed by both ¹H and ¹³C NMR spectroscopy, which showed the disappearance of the benzoyl CH and NH signals and appearance of high field NH₂ broad singlet at *ca.* 4.6 ppm. Amino acids 17 and 18 could be obtained from 13 and 15 in good yields by treatment with ammonia solution (Scheme 3).

Reduction of cyclohexene

Cyclohexene 13 was quantitatively hydrogenated in MeOH at room temperature, using 10% palladium/carbon as a catalyst to give cyclohexane 19, which is the direct precursor of the cyclohexane amino acid 20 (Scheme 4). The chemical shift of the CH=CH group of the former cyclohexene (compound 13) disappeared with appearance of new high field signals at 1.6 and 1.8 ppm of two methylene groups (compound 20) upon reduction. The ¹³C NMR spectrum showed new signals at approximately 25 ppm for the new methylene carbons of compound 20.

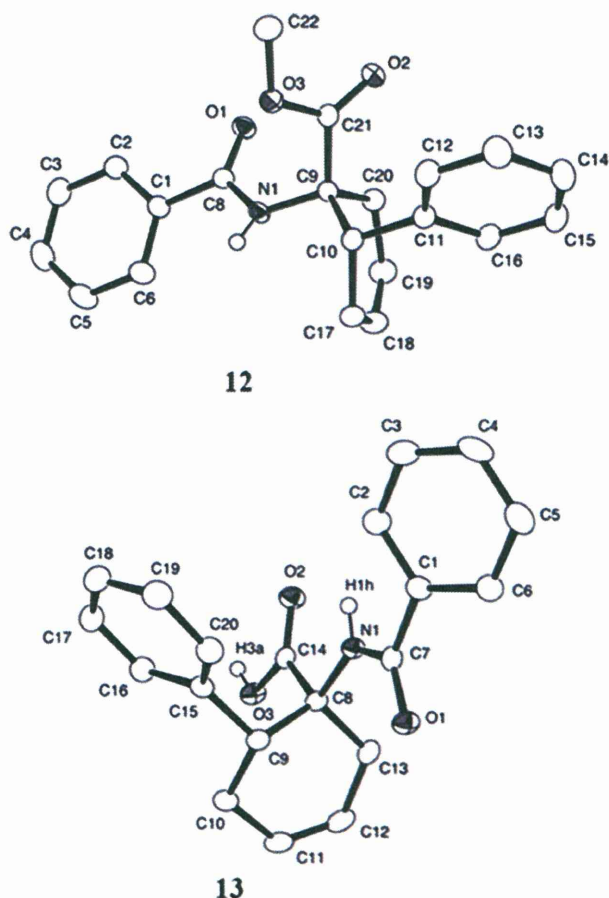
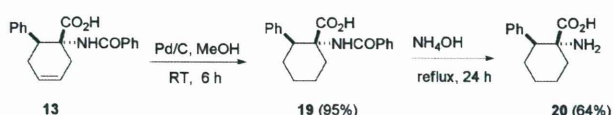
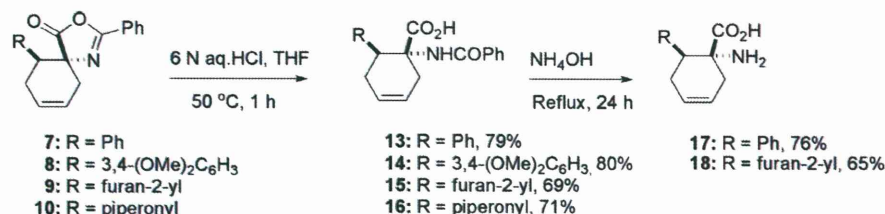


Fig. 2 X-Ray crystal structures of 12 and 13. Thermal probability ellipsoids are drawn at the 50% probability level (hydrogen atoms are omitted for clarity).



Scheme 4 Reduction of cyclohexene 13.

Azlactones and amino acids have characteristic stretching modes that are suitable for study by IR spectroscopy. The IR spectra of 3a–j contained weak and strong absorption bands located at *ca.* 1654, 1778, and 1816 cm⁻¹, which could be attributed to the vibrational modes of the C=C, C=N and C=O groups, respectively. These bands were not sensitive to the metathesis reactions in compounds 7–11. However, hydrolysis of azlactone followed by debenzoylation led to the complete disappearance of



Scheme 3 Conversion of azlactones to cyclic amino acids.

Table 3 Details of crystallographic data collection for **9**, **12** and **13**

	9	12	13
Formula	C ₁₈ H ₁₅ NO ₃	C ₂₂ H ₂₁ NO ₃	C ₂₀ H ₁₉ NO ₃
Fw	293.31	347.40	321.36
Crystal system	Orthorhombic	Monoclinic	Monoclinic
Space group	Fdd2	P2 ₁ /c	C2/c
<i>a</i> /Å	18.004(3)	10.6098(13)	29.149(6)
<i>b</i> /Å	39.249(6)	18.036(2)	7.5081(15)
<i>c</i> /Å	8.1408(11)	9.5122(12)	15.387(3)
α (°)	90	90	90
β (°)	90	98.7510(10)	107.300(2)
γ (°)	90	90	90
<i>V</i> /nm ³	5.7526(14)	1.7991(4)	3.2152(11)
<i>Z</i>	16	4	8
<i>D_c</i> /g cm ⁻³	1.355	1.283	1.328
<i>F</i> (000)	2464	736	1360
μ /mm ⁻¹	0.093	0.085	0.089
λ /Å	0.71073	0.71073	0.71073
Range (2 θ) for data collection/°	2.08–27.57	2.25–27.46	2.77–27.52
GOF	1.675	1.027	1.03
<i>T</i> /K	123	123	123
<i>R</i> ₁ ^a (<i>I</i> > 2 σ (<i>I</i>))	0.0391	0.0403	0.0448
w <i>R</i> ₂ ^b (<i>I</i> > 2 σ (<i>I</i>))	0.0546	0.0985	0.0954
<i>R</i> ₁ ^a (all data)	0.0476	0.0495	0.0693
w <i>R</i> ₂ ^b (all data)	0.0557	0.1039	0.1059

$$^a R_1 = \frac{\sum ||F_o| - |F_c||}{\sum |F_o|}, \quad ^b wR_2 = \left[\frac{\sum w(F_o^2 - F_c^2)^2}{\sum w(F_o^2)^2} \right]^{1/2}$$

the vibrational mode of C=N in the IR spectra of compounds **7–11**, which was replaced with a new strong absorption band (compounds **17**, **18** and **20**) at *ca.* 3500 cm⁻¹, which is characteristic of the NH₂ group, whereas ν (C=O) is shifted from *ca.* 1816 to 1725 cm⁻¹.

Conclusion

We have developed a procedure for the bis-allylation of activated azlactones *via* the three-component assembling reaction between arylidene azlactones, trifluoroborate and allyl acetate in the presence of palladium catalysts. In combination with our previously reported methodologies on the activated olefins, this methodology provides a novel process for the 1,2-bisfunctionalization of activated C=C bonds. This method allows an efficient synthesis of various 1,7-diene derivatives in good to excellent yields. The present catalytic reaction proceeds with various substituted azlactones. Metathesis cyclization of the resulting bis-allylated azlactones yielded the corresponding 3-oxa-1-aza-spiro[4.5]deca-1,7-dienes which could be either hydrolysed to the corresponding cyclohexenyl α -amino acids or reduced to the corresponding cyclohexenyl α -amino acids.

Experimental section

Materials and methods

Most chemicals and solvents were of analytical grade and used without further purification. Aldehydes and Grubbs' catalyst were commercially available. Starting materials **1**, **2a–h** and **2i–j** were prepared as described in the literature.^{22,47,48} NMR spectra (¹H and ¹³C) were measured on 400 MHz spectrometer. Chemical shifts of ¹H NMR and ¹³C NMR were expressed in parts per million (ppm, δ units), and coupling constant (*J*) values were expressed in units

of hertz (Hz). IR (cm⁻¹) spectra were determined as KBr disc on an FTIR-8600PC spectrometer. Electron spray ionization (ESI) mass spectra were recorded on an LCMS-2010 eV spectrometer. Elemental analyses were performed by 2400 automatic elemental analyzer. All compounds gave elemental analysis within $\pm 0.4\%$ of the theoretical values. Analytical thin layer chromatography (TLC) was performed on glass plates of silica gel 60 GF₂₅₄. Visualization was accompanied by UV light (254 nm), I₂ or KMnO₄. Melting points (mp) were determined on ATM-01 melting point apparatus. Preparative TLC was carried out using 0.75 mm layers of silica gel 60 GF₂₅₄ made from water slurries on glass plates of dimensions 20 \times 20 cm², followed by drying in air at 100 °C.

General procedure of amphiphilic bis-allylation of azlactone **2**

To a solution of azlactone **2** (0.65 mmol), allyltrifluoroborate (145 mg, 0.98 mmol), and Pd(dba)₃·CHCl₃ (35 mg, 0.033 mmol) in THF (10 ml) was added allyl acetate (2.1 ml, 1.96 mmol) and tricyclohexylphosphine (18 mg, 0.066 mmol) under nitrogen. The reaction mixture was heated with stirring at 70 °C for 24–48 h (TLC). The reaction was quenched with water, and the reaction mixture was extracted with ether, dried over anhydrous magnesium sulphate, and concentrated. Purification by preparative TLC with *n*-hexane/ethylacetate (9 : 1) as eluent gave the major diastereomer of bis-allylated product as a yellow oil.

Allyl-2-phenyl-4-(1-phenyl-but-3-enyl)-4H-oxazol-5-one (3a). Yield (97 mg, 45%); yellow oil; *R*_f 0.37 (*n*-hexane/AcOEt = 9 : 1); ¹H NMR (400 MHz, CDCl₃) δ 8.03 (d, 2H, *J* = 7.2 Hz), 7.57–7.28 (m, 8H), 5.45 (m, 2H), 5.02 (dd, 2H, *J* = 8 Hz, *J* = 3.5 Hz), 4.83 (dd, 2H, *J* = 8.0 Hz, *J* = 3.5 Hz), 3.18 (dd, 1H, *J* = 4.0 Hz, *J* = 4.0 Hz), 2.43 (m, 2H), 2.27 (m, 2H); ¹³C NMR (100 MHz, CDCl₃) δ 180.3, 160.2, 138.7, 135.2, 132.7, 130.5, 129.7, 128.8, 128.3, 128.0, 127.4, 125.8, 120.7, 117.1, 76.7, 52.1, 40.7, 36.2; IR (KBr disc) 3062, 2931, 1816, 1778, 1654, 972, 883, 702 cm⁻¹; MS, *m/z*

(ESI) 332.41 [100, M + 1]⁺; Anal. Calc. for C₂₂H₂₁NO₂: C, 79.73; H, 6.39; N, 4.23%. Found: C, 79.73; H, 6.32; N, 4.18%. ¹H NMR (400 MHz, CDCl₃) of the minor diastereomer: δ 7.98 (d, 2H, *J* = 7.00 Hz), 7.55–7.13 (m, 8H), 5.61 (m, 2H), 5.14 (dd, 2H, *J* = 8 Hz, *J* = 3.5 Hz), 4.95 (t, 2H, *J* = 7.5 Hz), 3.17 (dd, 1H, *J* = 4.0 Hz, *J* = 4.0 Hz), 2.67 (m, 2H), 2.51 (m, 2H).

4-Allyl-4-[1-(4-methoxy-phenyl)-but-3-enyl]-2-phenyl-4H-oxazol-5-one (3b). Yield (136 mg, 58%); yellow oil; *R*_f 0.53 (n-hexane/AcOEt = 9:1); ¹H NMR (400 MHz, CDCl₃) δ = 8.01 (d, 2H, *J* = 8.2 Hz), 7.55–7.43 (m, 3H), 7.38 (m, 2H), 7.23 (m, 2H), 5.49 (m, 2H), 5.16 (t, 2H, *J* = 10.5 Hz), 4.78 (t, 2H, *J* = 10.3 Hz), 3.75 (s, 3H), 3.23 (m, 1H), 2.43 (m, 2H), 2.23 (m, 2H); ¹³C NMR (100 MHz, CDCl₃) δ = 180.0, 162.3, 149.2, 147.7, 137.8, 136.6, 133.6, 129.4, 128.3, 128.3, 127.4, 125.6, 121.7, 115.0, 76.9, 55.8, 53.7, 39.4, 37.2; IR (KBr disc) 3065, 2935, 1808, 1774, 1655, 976, 885, 705 cm⁻¹; MS, *m/z* (ESI) 362.43 [100, M + 1]⁺; Anal. Calc. for C₂₃H₂₃NO₃: C, 76.43; H, 6.41; N, 3.88%. found: C, 76.32; H, 6.37; N, 3.79%. ¹H NMR (400 MHz, CDCl₃) of the minor diastereomer: δ = 7.90 (d, 2H, *J* = 8.0 Hz), 7.41–7.35 (m, 3H), 7.36 (m, 2H), 7.22 (m, 2H), 5.54 (m, 2H), 5.23 (t, 2H, *J* = 10.5 Hz), 4.71 (t, 2H, *J* = 10.3 Hz), 3.75 (s, 3H), 3.29 (m, 1H), 2.73 (m, 2H), 2.52 (m, 2H).

4-Allyl-4-[1-(3,4-dimethoxy-phenyl)-but-3-enyl]-2-phenyl-4H-oxazol-5-one (3c). Yield (170 mg, 67%); yellow oil; *R*_f 0.43 (n-hexane/AcOEt = 9:1); ¹H NMR (400 MHz, CDCl₃) δ = 8.03 (dd, 2H, *J* = 1.5 Hz, *J* = 1.5 Hz), 7.93 (d, 1H, *J* = 6.5 Hz), 7.57–7.49 (m, 3H), 6.84 (d, 1H, *J* = 8.0 Hz), 6.70 (m, 1H), 5.51 (m, 2H), 5.02 (t, 2H, *J* = 10.0 Hz), 4.86 (t, 2H, *J* = 10.0 Hz), 3.92 (s, 3H), 3.86 (s, 3H), 3.15 (m, 1H), 2.41 (m, 2H), 2.25 (m, 2H); ¹³C NMR (100 MHz, CDCl₃) δ = 179.3, 166.2, 149.2, 147.7, 137.6, 136.8, 133.1, 129.7, 128.8, 128.3, 127.4, 125.8, 121.6, 115.2, 77.0, 55.4, 55.2, 53.7, 39.5, 37.9; IR (KBr disc) 3058, 2936, 1812, 1772, 1655, 970, 882, 742 cm⁻¹; MS, *m/z* (ESI) 392.46 [100, M + 1]⁺; Anal. Calc. for C₂₄H₂₃NO₄: C, 73.64; H, 6.44; N, 3.58%. found: C, 73.59; H, 6.39; N, 3.47%. ¹H NMR (400 MHz, CDCl₃) of the minor diastereomer: δ = 7.93 (d, 2H, *J* = 4 Hz), 7.90 (d, 1H, *J* = 6.5 Hz), 7.54–7.45 (m, 3H), 6.83 (d, 1H, *J* = 8.0 Hz), 6.68 (m, 1H), 5.71 (m, 2H), 5.14 (t, 2H, *J* = 10.0 Hz), 4.79 (t, 2H, *J* = 10.0 Hz), 3.92 (s, 3H), 3.85 (s, 3H), 3.28 (m, 1H), 2.77 (m, 2H), 2.46 (m, 2H).

4-Allyl-4-[1-(4-dimethylamino-phenyl)-but-3-enyl]-2-phenyl-4H-oxazol-5-one (3d). Yield (114 mg, 47%); yellow oil; *R*_f 0.6 (n-hexane/AcOEt = 9:1); ¹H NMR (400 MHz, CDCl₃) δ = 8.07 (d, 2H, *J* = 3.5 Hz), 7.91 (d, 1H, *J* = 4.0 Hz), 7.73–7.40 (m, 5H), 5.47 (m, 2H), 4.99 (t, 2H, *J* = 7.5 Hz), 4.83 (t, 2H, *J* = 7.5 Hz), 3.17 (m, 1H), 2.99 (s, 3H), 2.83 (s, 3H), 2.42 (m, 2H), 2.23 (m, 2H); ¹³C NMR (100 MHz, CDCl₃) δ = 179.2, 168.3, 146.8, 137.6, 135.8, 131.5, 130.0, 129.6, 128.4, 127.4, 114.8, 115.7, 78.6, 40.5, 40.1, 35.8; IR (KBr disc) 3060, 2934, 1815, 1775, 1656, 987, 880, 725 cm⁻¹; MS, *m/z* (ESI) 375.48 [100, M + 1]⁺; Anal. Calc. for C₂₄H₂₆N₂O₂: C, 76.98; H, 7.00; N, 7.48%. found: C, 76.92; H, 6.97; N, 7.43%. ¹H NMR (400 MHz, CDCl₃) of the minor diastereomer: δ = 7.93 (d, 2H, *J* = 3.5 Hz), 7.90 (d, 1H, *J* = 4.0 Hz), 7.70–7.42 (m, 5H), 5.82 (m, 2H), 4.93 (t, 2H, *J* = 7.5 Hz), 4.80 (t, 2H, *J* = 7.5 Hz), 3.25 (m, 1H), 3.00 (s, 3H), 2.82 (s, 3H), 2.53 (m, 2H), 2.31 (m, 2H).

4-Allyl-4-[1-(4-nitro-phenyl)-but-3-enyl]-2-phenyl-4H-oxazol-5-one (3e). Yield (120 mg, 49%); yellow oil; *R*_f 0.42 (n-hexane/AcOEt = 9:1); ¹H NMR (400 MHz, CDCl₃) δ = 8.21

(d, 2H, *J* = 8.0 Hz), 8.04 (d, 2H, *J* = 8.0 Hz), 7.66–7.51 (m, 5H), 5.47 (m, 2H), 5.06 (dd, 2H, *J* = 9.0 Hz, *J* = 8.5 Hz), 4.86 (dd, 2H, *J* = 10.4 Hz, *J* = 9.6 Hz), 3.32 (dd, 1H, *J* = 6.0 Hz, *J* = 4.8 Hz), 2.45 (m, 2H), 2.20 (m, 2H); ¹³C NMR (100 MHz, CDCl₃) δ = 179.4, 160.7, 147.3, 146.5, 134.0, 133.0, 130.6, 129.7, 128.8, 128.0, 125.4, 123.5, 121.2, 118.0, 76.7, 51.5, 40.6, 36.0; IR (KBr disc) 3061, 2939, 1820, 1771, 1652, 976, 885, 741 cm⁻¹. MS, *m/z* (ESI) 454 [100, M + 2K]⁺; Anal. Calc. for C₂₂H₂₀N₂O₄: C, 70.20; H, 5.36; N, 7.44%. found: C, 70.17; H, 5.33; N, 7.40%. ¹H NMR (400 MHz, CDCl₃) of the minor diastereomer: δ = 8.13 (d, 2H, *J* = 8.0 Hz), 8.07 (d, 2H, *J* = 8.0 Hz), 7.66–7.51 (m, 5H), 5.61 (m, 2H), 5.14 (dd, 2H, *J* = 9.0 Hz, *J* = 8.5 Hz), 4.84 (dd, 2H, *J* = 10.4 Hz, *J* = 9.6 Hz), 3.74 (dd, 1H, *J* = 6.0 Hz, *J* = 4.8 Hz), 2.84 (m, 2H), 2.61 (m, 2H).

4-Allyl-4-(1-(furan-2-yl)but-3-enyl)-2-phenyloxazol-5(4H)-one (3f). Yield (152 mg, 73%); yellow oil; *R*_f 0.77 (n-hexane/AcOEt = 9:1); ¹H NMR (400 MHz, CDCl₃) δ = 8.00 (d, 2H, *J*_{CH} = 10.0 Hz), 7.58–7.47 (m, 3H), 7.35 (d, 1 H, *J* = 8.0 Hz), 6.28 (d, 2H, *J* = 8.8 Hz), 5.57 (m, 2H), 5.12 (m, 2H), 4.85 (t, 2H, *J* = 10.0 Hz), 3.29 (m, 1H), 2.50 (m, 3H), 2.26 (m, 1H); ¹³C NMR (100 MHz, CDCl₃) δ = 178.4, 169.1, 157.7, 141.9, 137.6, 135.5, 131.4, 128.4, 115.7, 111.1, 105.7, 78.3, 43.5, 37.8, 29.6; IR (KBr) 3067, 2933, 1814, 1774, 1655, 973, 885, 719 cm⁻¹; MS, *m/z* (ESI) 321 [75, M]⁺; Anal. Calc. for C₂₀H₁₉NO₃: C, 74.75; H, 5.96; N, 4.36%. found: C, 74.62; H, 5.87; N, 4.27%. ¹H NMR (400 MHz, CDCl₃) of the minor diastereomer: δ = 7.96 (d, 2H, *J*_{CH} = 10.0 Hz), 7.56–7.48 (m, 3H), 7.31 (d, 1 H, *J* = 8.0 Hz), 6.17 (d, 2H, *J* = 8.8 Hz), 5.73 (m, 2H), 5.07 (m, 2H), 4.81 (t, 2H, *J* = 10.0 Hz), 3.31 (m, 1H), 2.62 (m, 3H), 2.41 (m, 1H).

4-Allyl-4-(1-benzo[1,3]dioxol-5-yl-but-3-enyl)-2-phenyl-4H-oxazol-5-one (3g). Yield (182 mg, 75%); yellow oil; *R*_f 0.35 (n-hexane/AcOEt = 9:1); ¹H NMR (400 MHz, CDCl₃) δ = 8.04 (d, 2H, *J* = 8.0 Hz), 7.57–7.44 (m, 3H), 6.81–6.61 (m, 3H), 5.94 (s, 2H), 5.49 (m, 2H), 5.02 (m, 2H), 4.85 (m, 2H), 3.09 (m, 1H), 2.39 (m, 2H), 2.32 (m, 2H); ¹³C NMR (100 MHz, CDCl₃) δ = 177.7, 169.0, 148.5, 146.1, 136.8, 136.0, 132.7, 129.5, 128.7, 128.2, 121.6, 115.7, 113.6, 102.4, 78.6, 42.6, 42.3, 32.0; IR (KBr) 3066, 2932, 1815, 1775, 1656, 976, 885, 723 cm⁻¹; MS, *m/z* (ESI) 375.42 [100, M + 1]⁺. Anal. Calc. for C₂₃H₂₁NO₄: C, 73.58; H, 5.64; N, 3.73%. found: C, 73.53; H, 5.59; N, 3.71%. ¹H NMR (400 MHz, CDCl₃) of the minor diastereomer: δ = 7.91 (d, 2H, *J* = 8.0 Hz), 7.56–7.45 (m, 3H), 6.73–6.60 (m, 3H), 5.82 (s, 2H), 5.67 (m, 2H), 5.00 (m, 2H), 4.81 (m, 2H), 3.15 (m, 1H), 2.84 (m, 2H), 2.65 (m, 2H).

4-Allyl-2-phenyl-4-(1-(pyridin-4-yl)but-3-enyl)oxazol-5(4H)-one (3h). Yield (133 mg, 62%); yellow oil; *R*_f 0.45 (n-hexane/AcOEt = 9:1); ¹H NMR (400 MHz, CDCl₃) δ = 8.75 (d, 2H, *J* = 8.5 Hz), 8.25 (d, 2H, *J* = 8.5 Hz), 8.0 (d, 2H, *J* = 8.5 Hz), 7.72 (m, 1H), 7.51 (m, 2H), 5.65 (m, 2H), 4.95 (m, 2H), 4.81 (m, 2H), 3.19 (m, 1H), 2.49, 2.30 (m, 4H); ¹³C NMR (100 MHz, CDCl₃) δ = 180.2, 160.1, 154.0, 149.1, 139.0, 135.0, 129.6, 128.4, 126.3, 120.9, 117.1, 76.8, 52.1, 40.7, 36.2; IR (KBr disc) 3065, 2932, 1817, 1771, 1653, 975, 886, 722 cm⁻¹; MS, *m/z* (ESI) 333.40 [100, M + 1]⁺; Anal. Calc. for C₂₁H₂₀N₂O₂: C, 75.88; H, 6.06; N, 8.43%. found: C, 75.84; H, 6.03; N, 8.40%. ¹H NMR (400 MHz, CDCl₃) of the minor diastereomer: δ = 8.73 (d, 2H, *J* = 8.5 Hz), 8.25 (d, 2H, *J* = 8.5 Hz), 8.1 (d, 2H, *J* = 8.5 Hz), 7.68 (m, 1H), 7.53 (m, 2H), 5.74

(m, 2H), 5.06 (m, 2H), 4.92 (m, 2H), 3.27 (m, 1H), 2.64, 2.45 (m, 4H).

(E/Z)-4-allyl-2-phenyl-4-(1-phenylhexa-1,5-dien-3-yl)oxazol-5(4H)-one (3i). Yield (74 mg, 32%); yellow oil; R_f 0.5 (n-hexane/AcOEt = 9:1); $^1\text{H NMR}$ (400 MHz, CDCl_3) δ = 8.02 (d, 2H, J = 7.0 Hz), 7.61–7.21 (m, 8H), 6.55 (m, 1H), 6.21 (m, 1H), 5.63 (m, 2H), 5.12 (m, 4H), 3.31 (m, 1H), 2.75 (m, 2H), 2.45 (m, 2H); $^{13}\text{C NMR}$ (100 MHz, CDCl_3) δ = 179.8, 160.4, 136.7, 135.2, 134.4, 132.7, 130.5, 128.8, 128.5, 128.5, 128.0, 127.6, 127.3, 126.5, 126.4, 125.8, 120.7, 117.0, 76.5, 50.0, 40.7, 35.0; IR (KBr disc) 3065, 2937, 1815, 1778, 1659, 972, 886, 735 cm^{-1} ; MS, m/z (ESI) 356 [100, M - 1] $^+$; Anal. Calc. for $\text{C}_{24}\text{H}_{23}\text{NO}_2$: C, 80.64; H, 6.49; N, 3.92%. found: C, 80.59; H, 6.47; N, 3.87%. $^1\text{H NMR}$ (400 MHz, CDCl_3) of the minor diastereomer: δ = 8.00 (d, 2H, J = 7.0 Hz), 7.60–7.23 (m, 8H), 6.73 (m, 1H), 6.30 (m, 1H), 5.71 (m, 2H), 5.19 (m, 4H), 3.43 (m, 1H), 2.83 (m, 2H), 2.64 (m, 2H).

4-Allyl-4-(1-cyclohexylbut-3-enyl)-2-phenyloxazol-5(4H)-one (3j). Yield (138 mg, 63%); yellow oil; R_f 0.6 (n-hexane/AcOEt = 9:1); $^1\text{H NMR}$ (400 MHz, CDCl_3) δ = 8.04 (m, 2H), 7.64–7.41 (m, 3H), 5.53 (m, 2H), 5.02 (m, 2H), 4.86 (m, 2H), 3.26 (m, 1H), 2.97 (t, 1H, J = 10.0 Hz), 2.62, 2.38 (m, 4H), 2.23, 1.95 (m, 3H), 1.71–1.49 (m, 4H); $^{13}\text{C NMR}$ (100 MHz, CDCl_3) δ = 176.5, 167.2, 137.9, 136.1, 131.3, 128.4, 115.8, 76.5, 41.5, 33.2, 31.7, 29.4, 28.4, 28.3, 26.8; IR (KBr disc) 3062, 2939, 1822, 1779, 1656, 975, 887, 741 cm^{-1} ; MS, m/z (ESI) 337 [100, M] $^+$; Anal. Calc. for $\text{C}_{22}\text{H}_{27}\text{NO}_2$: C, 78.30; H, 8.06; N, 4.15%. found: C, 78.27; H, 8.03; N, 4.11%. $^1\text{H NMR}$ (400 MHz, CDCl_3) of the minor diastereomer: δ = 7.87 (m, 2H), 7.63–7.40 (m, 3H), 5.76 (m, 2H), 5.14 (m, 2H), 4.88 (m, 2H), 3.37 (m, 1H), 3.11 (t, 1H, J = 10.0 Hz), 2.83, 2.46 (m, 4H), 2.35, 2.06 (m, 3H), 1.82–1.68 (m, 4H).

General procedure for ring closing diene metathesis: synthesis of cyclohexene derivatives (7–11)

The typical procedure for the ring closing diene metathesis is as follows: precursor diene **3c**, **3f**, **3g**, or **3j** (1 mmol) was dissolved in freshly distilled and degassed dichloromethane (17 mL) under a nitrogen atmosphere. After stirring for 10 min at room temperature, ruthenium catalyst 1st generation (41.2 mg, 0.05 mmol) dissolved in dichloromethane (3 mL) was added by syringe. After 5–8 h of reflux at 40 °C, the reaction was complete as indicated by TLC. The solution was concentrated *via* rotavapor. TLC of the crude oil gave the corresponding cyclohexene derivatives as white solids.

2,10-Diphenyl-3-oxa-1-aza-spiro[4.5]deca-1,7-dien-4-one (7). Yield (257 mg, 85%); white solid; R_f 0.2 (n-hexane/AcOEt = 9:1); mp = 140–142 °C; $^1\text{H NMR}$ (300 MHz, CDCl_3) δ = 7.75 (d, 2H, J = 6.0 Hz), 7.46–7.10 (m, 8H), 6.04 (bs, 1H), 5.79 (bs, 1H), 3.45 (t, 1H, J = 6.6 Hz), 3.08 (t, 1H, J = 15.0 Hz), 2.90 (d, 1H, J = 18.0 Hz), 2.45 (t, 2H, J = 18.0 Hz); $^{13}\text{C NMR}$ (100 MHz, CDCl_3) δ = 177.0, 161.0, 138.4, 136.4, 131.6, 128.6, 126.7, 68.5, 39.0, 34.2, 27.6; IR (KBr disc) 3065, 2935, 1825, 1775, 1658, 1045, 887, 742 cm^{-1} ; MS, m/z (ESI) 304 [100, M + 1] $^+$. Anal. Calc. for $\text{C}_{20}\text{H}_{17}\text{NO}_2$: C, 79.19; H, 5.65; N, 4.62%. found: C, 79.11; H, 5.58; N, 4.57%.

10-(3,4-Dimethoxy-phenyl)-2-phenyl-3-oxa-1-aza-spiro[4.5]deca-1,7-dien-4-one (8). Yield (315 mg, 87%); white solid; R_f 0.15

(n-hexane/AcOEt = 9:1); mp = 134–136 °C; $^1\text{H NMR}$ (400 MHz, CDCl_3) δ = 7.76 (t, 2H, J = 6.5 Hz), 7.47–7.34 (m, 4H), 6.79–6.69 (m, 2H), 6.05 (m, 1H), 5.68 (m, 1H), 3.78 (s, 3H), 3.74 (s, 3H), 3.40 (dd, 1H, J = 6.0, 6.5 Hz), 3.05 (t, 1H, J = 12.0 Hz), 2.85 (m, 1H), 2.43 (t, 2H, J = 12.0 Hz); $^{13}\text{C NMR}$ (100 MHz, CDCl_3) δ = 177.0, 163.2, 147.6, 146.0, 136.4, 132.0, 128.6, 126.3, 115.8, 68.2, 54.5, 40.0, 33.8, 27.4; IR (KBr disc) 3059, 2928, 1810, 1775, 1652, 1025, 887, 738 cm^{-1} ; MS, m/z (ESI) 364 [100, M + 1] $^+$; Anal. Calc. for $\text{C}_{22}\text{H}_{21}\text{NO}_4$: C, 72.71; H, 5.82; N, 3.85%. found: C, 72.63; H, 5.77; N, 3.81%.

10-Furan-2-yl-2-phenyl-3-oxa-1-aza-spiro[4.5]deca-1,7-dien-4-one (9). Yield (269 mg, 92%); white solid; R_f 0.25 (n-hexane/AcOEt = 9:1); mp = 131–133 °C; $^1\text{H NMR}$ (400 MHz, CDCl_3) δ = 7.86 (d, 2H, J = 8 Hz), 7.52–7.49 (m, 1H), 7.43–7.40 (m, 2H), 7.18 (s, 1H), 6.15 (dd, 2H, J = 8.0, 6.5 Hz), 5.96 (m, 1H), 5.73 (m, 1H), 3.55 (t, 1H, J = 10.0 Hz), 2.95 (t, 1H, J = 12.0 Hz), 2.78 (d, 1H, J = 12.5 Hz), 2.42 (m, 2H); $^{13}\text{C NMR}$ (100 MHz, CDCl_3) δ = 177.2, 161.5, 153.3, 141.7, 132.6, 128.6, 127.8, 127.0, 125.7, 121.2, 110.0, 106.0, 69.4, 40.0, 33.7, 27.3; IR (KBr disc) 3057, 2932, 1821, 1775, 1656, 975, 889, 729 cm^{-1} ; MS, m/z (ESI) 295 [100, M + 2H] $^+$; Anal. Calc. for $\text{C}_{18}\text{H}_{15}\text{NO}_3$: C, 73.71; H, 5.15; N, 4.78%. found: C, 73.68; H, 5.11; N, 4.75%.

10-Benzo[1,3]dioxol-5-yl-2-phenyl-3-oxa-1-aza-spiro[4.5]deca-1,7-dien-4-one (10). Yield (263 mg, 76%); white solid; R_f 0.3 (n-hexane/AcOEt = 9:1); mp = 165–167 °C; $^1\text{H NMR}$ (400 MHz, CDCl_3) δ = 7.97 (m, 2H), 7.46–7.34 (m, 4H), 6.72–6.53 (m, 3H), 6.02 (m, 1H), 5.87 (m, 2H), 5.72 (m, 1H), 3.37 (q, 1H, J = 8.0 Hz), 2.96 (t, 1H, J = 11.5 Hz), 2.79 (d, 1H, J = 11.5 Hz), 2.39 (m, 2H); $^{13}\text{C NMR}$ (100 MHz, CDCl_3) δ = 178.0, 162.8, 148.0, 146.7, 136.6, 135.7, 132.6, 129.6, 128.9, 121.3, 115.7, 113.4, 101.8, 68.5, 40.6, 36.0, 28.0; IR (KBr disc) 3065, 2935, 1813, 1772, 1654, 972, 885, 725 cm^{-1} ; MS, m/z (ESI) 347 [100, M] $^+$; Anal. Calc. for $\text{C}_{20}\text{H}_{17}\text{NO}_4$: C, 72.61; H, 4.93; N, 4.03%. found: C, 72.58; H, 4.88; N, 3.99%.

2-Phenyl-10-styryl-3-oxa-1-aza-spiro[4.5]deca-1,7-dien-4-one (11). Yield (230 mg, 70%); white solid; R_f 0.28 (n-hexane/AcOEt = 9:1); mp = 172–174 °C; $^1\text{H NMR}$ (400 MHz, CDCl_3) δ = 7.94 (m, 2H), 7.54–7.41 (m, 3H), 7.22–7.15 (m, 5H), 6.54 (m, 1H), 5.94 (m, 2H), 5.73 (m, 1H), 2.96 (m, 1H), 2.64 (m, 2H), 2.44 (m, 2H); $^{13}\text{C NMR}$ (100 MHz, CDCl_3) δ = 177.8, 160.3, 136.8, 134.1, 133.7, 129.0, 128.7, 128.4, 128.1, 126.5, 126.4, 126.3, 125.8, 122.0, 121.3, 69.7, 43.5, 42.9, 34.5, 32.8, 28.5, 27.7; IR (KBr disc) 3068, 2932, 1815, 1775, 1656, 977, 889, 741 cm^{-1} ; MS, m/z (ESI) 352 [100, M + Na] $^+$; Anal. Calc. for $\text{C}_{22}\text{H}_{19}\text{NO}_2$: C, 80.22; H, 5.81; N, 4.25%. found: C, 80.19; H, 5.79; N, 4.21%.

General procedure of hydrolysis of azlactones

Method A. 6 N aq. HCl (10 mL) was added to a solution of azlactone **7** (303 mg, 1 mmol) in 10 mL methanol at room temperature in a 50 mL round flask. The reaction mixture was heated at 50 °C for 1 h and the formation of the products was monitored by TLC. The solvents were evaporated under vacuum to yield a white solid of the crude product which was purified by preparative TLC using CH_2Cl_2 /methanol (90:5) as eluent to yield colorless crystalline solids.